HOST UNIVERSITY: Lund University

FACULTY: Faculty of Engineering

DEPARTMENT: Division of Fire Safety Engineering

Academic Year 2019-2020

INTERMEDIATE-SCALE TESTS AND CONE CALORIMETER TESTS – FIRE BEHAVIOUR OF SELECTED FAÇADE MATERIALS

Tanja Černoša

Promoters:

Patrick Van Hees, Lund University

Roy Weghorst, Kingspan

Master thesis submitted in the Erasmus Mundus Study Programme

International Master of Science in Fire Safety Engineering

DISCLAIMER

This thesis is submitted in partial fulfilment of the requirements for the degree of *The International Master of Science in Fire Safety Engineering (IMFSE)*. This thesis has never been submitted for any degree or examination to any other University/programme. The author(s) declare(s) that this thesis is original work except where stated. This declaration constitutes an assertion that full and accurate references and citations have been included for all material, directly included and indirectly contributing to the thesis. The author(s) gives (give) permission to make this master thesis available for consultation and to copy parts of this master thesis for personal use. In the case of any other use, the limitations of the copyright have to be respected, in particular with regard to the obligation to state expressly the source when quoting results from this master thesis. The thesis supervisor must be informed when data or results are used.

Read and approved,

Tanja Černoša

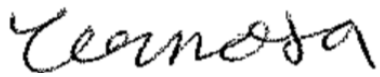

30th April 2020

Abstract

In the last few years, the implementation of well-ventilated façades in buildings increased due to their improved energy performance. However, their double-wall construction due to the limited airflow within an air cavity represents a significant fire risk, since the flames that spread into the air cavity can elongate up to ten times.

The main goal of this thesis is to provide additional information regarding the fire behaviour of stone wool, phenolic foam, as well as the stone wool and WRB composite, that are frequently installed materials in the well-ventilated façade systems. Their fire behaviour was initially evaluated with the cone calorimeter and then compared to the results of the intermediate-scale façade tests.

The heat release rates that were obtained for the test, including the WRB and stone wool material demonstrated, that the cone calorimeter data is comparable to intermediate-scale test. Based on the cone calorimeter results, the WRB and stone wool composite will have relatively quick ignition time at various heat flux values. For this reason, the WRB and stone wool could represent a fire hazard when implemented in a façade system. In addition, the intermediate-scale experiments also exhibited the significance of additional parameters on the heat release rates, such as oxygen availability and the instalment of the cavity barriers.

Povzetek

V zadnjih letih se pri gradnji zaradi svojih dobrih energetskih sposobnosti vedno več uporabljajo tako imenovane prezračevane fasade. Sama konstrukcija teh fasad je sestavljena iz dveh delov, med katerima se nahaja zračna plast. Zaradi omejene količine zraka v zračni plasti pa predstavlja prezračevana fasada tudi veliko tveganje za požar, saj se dolžina le-tega v primeru širjenja ognja v zračno plast lahko podaljša do desetkrat.

Glavni cilj raziskovalne naloge je bil pridobitev dodatnih informacij o požarnih lastnostih materialov, ki se pogosto uporabljajo v prezračevalnih fasadah: kamene volne, fenolične pene in kompozita, sestavljenega iz kamene volne in vodoodporne membrane. Najprej smo ocenili požarne lastnosti teh materialov v stožčastem kalorimetru, nato pa smo pridobljene rezultate primerjali še podatki preskusov fasad (t.i. intermediate-scale façade tests).

Tekom raziskave smo ugotovili, da je bilo sproščanje toplote ob testiranju kompozita v stožčastem kalorimetru primerljivo s preskusom fasade. Glede na rezultate pridobljene s stožčastim kalorimetrom, kompozit sestavljen iz kamene volne in vodoodporne membrane ima hiter čas vžiga. Prav tako smo ugotovili, da na stopnjo sproščene toplote pri preskusih fasad vpliva tudi dodatni parametri kot sta količina zraka v fasadi in postavitev barier v zračni plasti.

IMFSE Master Thesis Declaration

This form has been developed in the context of the unforeseen circumstances due to Covid-19, necessitating a reduction of practical project work (whether it be laboratory based, computational, or fieldwork) during the master thesis semester. It acts as a record of the impact on the master thesis. The form has been completed by the student and verified by the supervisor. **A copy of the signed form is included behind the abstract in the dissertation.**

Name: Tanja Černoša _____

Work completed

All items of wholly, or partially completed work must be listed, indicating the percentage completion for each task. **Please take care to provide a full detailed list of all work done.**

The initial plan for the thesis was to execute nine intermediate-scale façade tests, composed of three different material compositions that would be tested at three different cavity widths. In all the nine experiments, the air availability within the tests would initially be determined based on the experimental results of Daniel Fogerty that would demonstrate the flame spread within the air cavity.
However, due to the pandemic of Coronavirus and closure of the fire laboratory, the plan modified to a combination of small scale and intermediate-scale experiments that are not based on the influence of air availability within the tests.
In this experimental thesis, the work that has been completed includes 11 cone calorimeter tests and three intermediate-scale façade tests. Therefore, the total percentage of completion is estimated to be at 33.3%.

Work not commenced

Any items of outstanding work that have not been started should be listed here.

The work that hasn't started is the construction and execution of six intermediate-scale façade tests.

Declaration

To the best of our knowledge, this form is an accurate record of the project status on 27.04.2020.

Student: _____ (Signature)

Patrick van Hees

Supervisor: _____

Acknowledgements

I want to thank my supervisor, professor Patrick Van Hees for all the support and guidance throughout this final semester. There have been many challenges on the way; however, his continuous help in finding alternative solutions for the experimental part of the thesis has truly been appreciated.

I would also like to thank Roy Weghorst for the opportunity of executing this experimental thesis provided by Kingspan. His knowledge and help with the experimental part of the thesis, especially with the construction of the intermediate-scale tests have been a very valuable experience.

A special thank you also goes to the employees at FireSERT, Ulster University, that helped with the execution of the intermediate-scale tests. I want to thank especially Maurice McKee, who provided the experimental data for the analysis of the tests.

For the execution of the cone calorimeter tests at Lund University, I would like to thank Dan Madsen that helped me not only with the completion of the experiments but also with the suggestions on improving the test data.

The last two years have been an adventure which was composed of ups and downs. I want to thank my family as well as my friends that supported me throughout this journey and encouraged me to do my best. However, I cannot imagine spending these two years without my newly acquired IMFSE friends to share all the moments with. For this reason, thank you for all the “coffee breaks” during the late-night study groups, and for all those plans we are going to do together after submitting that “final report”.

List of abbreviations

ETICS – EXTERNAL THERMAL INSULATION COMPOSITE SYSTEM

EIFS – EXTERIOR INSULATION FINISHING SYSTEM

WRB – WATER-RESISTIVE BARRIER

PIR – POLYISOCYANURATE

ACM – ALUMINIUM COMPOSITE MATERIAL

HPL – HIGH-PRESSURE LAMINATE

MCM – METAL COMPOSITE CLADDING

PE – POLYETHYLENE

ACM-PE – ALUMINIUM COMPOSITE MATERIAL WITH A CORE MATERIAL OF POLYETHYLENE

ACM-FR – ALUMINIUM COMPOSITE MATERIAL WITH A CORE MATERIAL THAT IS OF 70% NON-COMBUSTIBLE MATERIAL

ACM-A2 – ALUMINIUM COMPOSITE MATERIAL WITH A CORE MATERIAL THAT IS OF 90% NON-COMBUSTIBLE MATERIAL

TGA – THERMOGRAPHIC ANALYSIS

MCC – MICROSCALE COMBUSTION CALORIMETRY

TPE – THERMOPLASTIC ELASTOMERS

HRR – HEAT RELEASE RATE

NS – NATURAL STONE

CSB – CALCIUM SILICATE BOARD

Table of content

List of tables

List of figures

1. Introduction

The façade can be defined in various ways, that can either represent only an outer skin of the building or an entire exterior wall structure. In this thesis, the definition of the façade that is going to be considered is the following [1]:

"*A complete external wall construction of any type (massive wall or curtain wall..etc.) or constitution (masonry, combustible material …etc*)" *[1].*

The design of the façade system is influenced by various factors, such as the topography and site of the building that will determine the climate as well as its effect on the façade system. The design will be influenced by the technical requirements that include humidity, esthetical specifications, and insulation criteria. Furthermore, it will also be based on material availability, including their thermal characteristics and the architectural features of the building [2,3]. The materials that were traditionally used in a façade, particularly brick or stone with higher thermal capacities, provided poor control of indoor temperature [4]. For this reason, a substantial amount of energy was lost through the façade [5,6]. In recent years the demand for a more energy-efficient façade has increased to provide more sustainable buildings since structures in Europe represent approximately 40% of the total energy consumption [5–7]. The energy losses have been reduced by implementing new lightweight energy-efficient materials on the façades of new and existing buildings [5,6]. The implementation of new materials improved the thermal insulation of the building; however, many of the applied materials were combustible [4,6].

In the last decade, there were several façade fires where the fire spread along the façade due to the applied combustible materials [2,6]. Façades are representing a critical element in a building because the fire can not be extinguished by active protection systems implemented within a building [6]. For this reason, the façade fires, especially in high-rise buildings, represent a challenge for the emergency services and the evacuation of a large number of occupants [2,6].

The façade fires can occur in various ways; however, a fire frequently propagates into the façade system from initial fire sources. The fire that starts inside of a building, specifically in a room can spread through the joint system of a façade from one level of a building to another as presented in Figure 1. However, the developing room fire can also result in a breakage of the window; therefore, the flame can spread through the window opening to the façade system and continue to the next floor level of the building [8,9]. On the other hand, the risk for the façade system do not only represent the fires that can begin inside of the building but as well the external fires that can either start next to the façade or in an adjacent building [10]. The fire that occurs near the exterior of the building can start as a container fire and can progress to the façade system through the void that is present between the façade and the

building exterior. In case the fire occurs in the adjacent building, the falling debris from the exterior of the building could potentially also ignite the façade system [9]. Different ways of fire propagation into the façade system can be observed in Figure 1. As already mentioned, the fire can either begin in a compartment or externally; however, the fire spread will be influenced by the combustibility of external cladding panels.

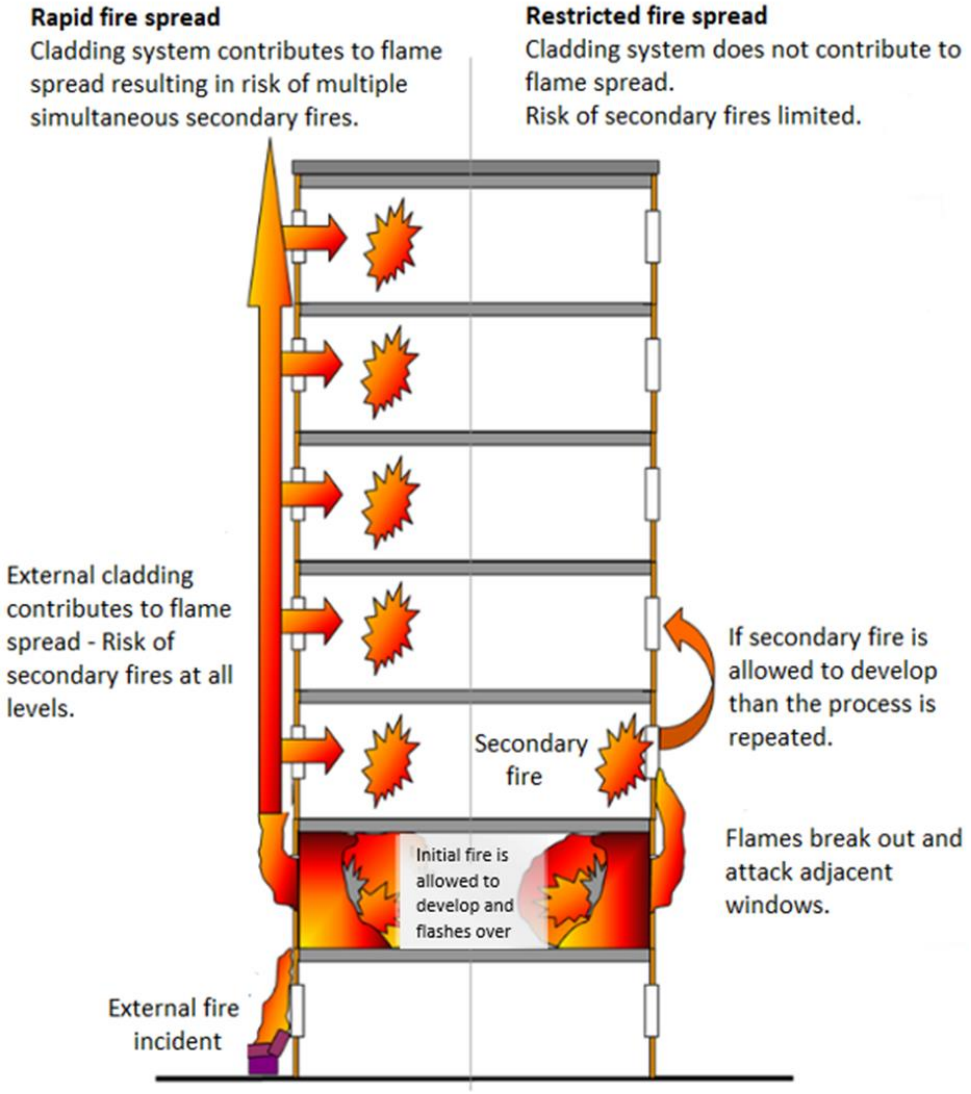

***Figure 1**: Possibilities of flame spread along the façade modified from [3,11]*

1.1 Type of façade systems

Façade systems can be fundamentally separated into non-ventilated, low-ventilated and well-ventilated systems. The low-ventilated systems are usually applied to a structure with masonry or concrete walls. The system consists of the insulation material being installed with anchors on the loadbearing walls, and external cladding applied over the insulation material as weather protection [3,11,12]. The external cladding panels are frequently composed of a cement-based material that can have implemented synthetic and plaster finishing layer. For the ventilation purposes of the structure, the air gap is added between the loadbearing wall and the insulation material, which prevents the transmission of moisture into the structure [3]**.** An example of non-ventilated systems is the External Thermal Insulation Composite System (ETICS) that can also be referred to in North America as the Exterior Insulation Finishing System (EIFS) [12,13]. The ETICS systems usually consist of the thermal insulation layer, a reinforcing mesh layer, as well as the base coat and optional finishing layer [12]. An example of an ETICS system and its components are presented in Figure 2.

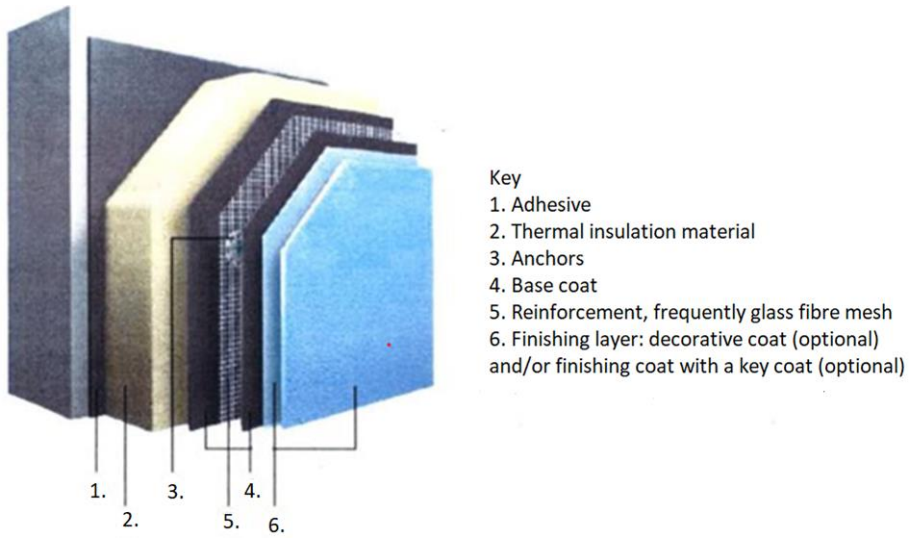

Figure 2*: An example of a non-ventilated façade (ETICS) modified from [3]*

The exterior cladding of the non-ventilated and low-ventilated façade systems is prone to rot and fungus, causing the materials within a façade to deteriorate [13,14]. For this reason, in the last decade, the implementation of well-ventilated façades in the new and existing buildings has increased. The systems are ventilated by a natural vertical flow of air through the cavity that prevents the occurrence of rot or fungus [14,15]. The well-ventilated façades are also designed to protect the structure against various weather conditions while improving the energy performance of the building [16]. The rainscreen cladding is the type of well-ventilated façade system and can sometimes also be referred to in the literature as the synonym for a well-ventilated façade [3,12].

The rainscreen cladding is a double-wall construction, composed of an external cladding panel followed by an air cavity and the exterior wall that is part of the existing building structure [17]. The insulation layer is usually installed on the exterior wall of the existing building and is exposed to the air cavity, that can transmit moisture to the insulation material [17–19]. For this reason, the insulation materials with high water permeability require a Water-Resistive Barrier (WRB) that protects the thermal insulation capacity of the material [19,20]. The external cladding panels are attached to the railing system and heated by the incident solar radiation that is consequently heating the air present in the cavity [11,14]. The well-ventilated façades generally have an air cavity that has a width of 20 to 100 mm, depending on the regulation [20]. The cavity enables air circulation between the external cladding panel and the wall of the existing structure by having the ventilation openings on the lower and upper side of the cavity that allow the ambient air to circulate using the buoyancy forces [15,17]. An example of a rainscreen cladding system is presented in Figure 3.

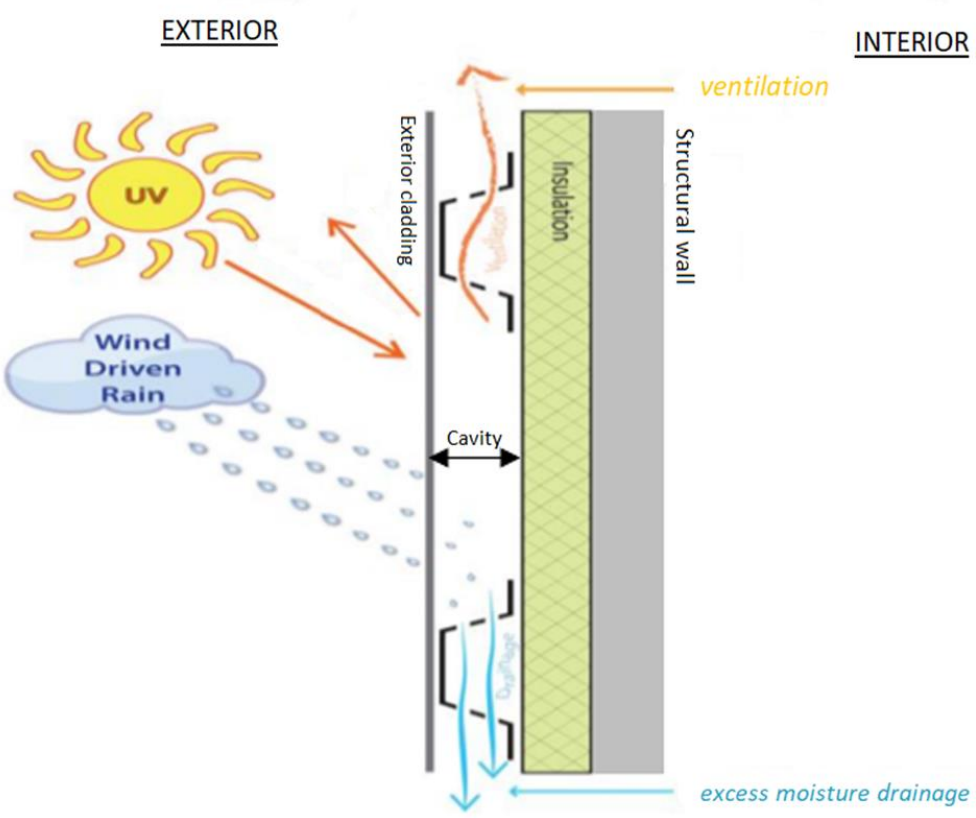

***Figure 3**: An example of a rainscreen cladding modified from [8]*

The air cavity does not only prevent the appearance of condensation and moisture damage on the façade, but it also enables lower energy consumption for heating and cooling of the building [15,17]. In the case of hot weather conditions, the external cladding is exposed to higher values of incident solar radiation; however, due to the presence of the air cavity, the amount of heat penetrating inside the building is reduced [17].

The well-ventilated façades represent several benefits due to the vertical flow of air present in the cavity defined as the “chimney effect” [15,17]. However, in the case of a fire spread inside of the cavity, due to the chimney effect, the flame can spread five to ten times the length that it has outside the cavity [7,11]. The flames will elongate, especially when confined entering the cavity because of the limited airflow and to support the combustion process [11,21]. Furthermore, the presence of the air cavity within the façade system also increases the energy released during the fire [22].

The vertical flame spread will represent a considerable risk for the floors above, mainly when the flame spread is not observed due to the external cladding panels. As a protection measure against the vertical flame spread within the cavity, the fire barriers are implemented in a horizontal orientation between the external cladding panels and the exterior wall. The horizontal fire barriers are allowing the air to propagate through the cavity; however, in case of a fire, the intumescent materials that are applied on the fire barriers seal the cavity and prevent the vertical flame spread [6,7]. The regulations regarding cavity barriers vary between the countries; therefore, in the UK, USA, and New Zealand cavity barriers are required; however, in Australia, the cavity barriers are not mandatory [12]. Nevertheless, even when the cavity barriers are implemented within the façade system, their performance is dependent on the fire behaviour of insulation material [23].

1.2 Classification of construction materials

The construction materials that are used in the European market are required to be tested and classified according to the Euroclass system. As part of the system, the materials are distributed into different classes based on their fire performance, according to EN 13501-1:2018, that evaluates their flammability characteristics**.** As it can be observed in Table 1, the materials are classified from A1 with no contribution to fire growth to class F that includes the products that can not be distributed in any other class [24]. Depending on the expected flammability characteristics of the material, different testing methods are employed to distribute the materials in the class from A1 to F [25]**.** An additional classification of materials regarding the smoke production was created that classifies materials from s1 with limited smoke production to s3 that has no limitations regarding smoke production. The materials also range from d0 to d2, depending on the occurrence of flaming droplets/particles during the fire. The class d0 represents the material without the flaming droplets/particles, d1 only has no flaming droplets/particles for a specific time period and d2 that has no limitations regarding the occurrence of flaming droplets/particles [24,26,27].

***Table 1**: Material classification and fire performance according to EN 13501-1:2018 [24]*

Class	Fire performance
A1	No contribution to the fire growth
A2	No significant contribution to the fire growth
B	Similar to class C but with more stringent requirements
C	Similar to class D but with more stringent requirements The product also has under the thermal attack by a single burning item a limited lateral spread of flame.
D	Products can resist a small flame attack for a longer period without substantial flame spread When undergoing thermal attack by a single burning item the product will have a sufficiently delayed and limited heat release
E	Products can resist a small flame attack for a short period without substantial flame spread
F	Products that can not be distributed in any other class

The regulations regarding the fire performance of material components that can be implemented inside of the façade system vary per country [28,29]. As an example, is presented the prescriptive guidance for England that defines the product requirements depending on their position within the façade system. The occupation of the buildings determines the required classification of the insulation material. For this reason, the buildings with a height of 18 m or more might be required to have the applied insulation materials on the façade of at least A2-s3,d2 or better. The material requirements regarding external cladding depend on the relevant boundary of the building that defines the shortest distance to the notional boundary. The external cladding that is applied to the façade that is less than 1000 mm from the relevant is required to be at least class B-s3,d2, or better. However, in case the relevant boundary is more than 1000 mm, the minimum material requirements are defined either as class C-s3,d2, or B class depending on the height and purpose of the building [28].

1.3 Properties of insulation materials

The insulation materials are categorized into organic and inorganic materials, with each of the groups being divided into natural and synthetic materials based on the applied processing methods [30]. In the European market, inorganic synthetic materials such as stone and glass wool represent approximately 60% of the market. On the other hand, organic polymeric materials account for around 30%, with the most frequently used organic polymeric material being polystyrene in various forms [31,32].

The most important property of insulation materials is thermal conductivity k, which represents the capacity of the material to transfer heat through the material. By defining the thermal conductivity of the material, the amount of heat losses can be estimated. Most of the insulating materials have the thermal conductivity in the range of 0.030 to 0.050 W/mK and lower the value of the thermal conductivity; the more insulating is the material. In case the material has thermal conductivity below 0.03 W/mK, it can be defined as excellent thermal performance. The heat conduction of the material is affected by the microstructure of the material its density as well as by the moisture content and temperature of the material. Insulation materials can also only withstand short periods of high temperatures without thermally decomposing, losing its form and strength [33]. The value of density defines the porosity of the material with low values representing porous materials that have high air permeability and, consequently, lower thermal conductivity [33,34]. The microstructure and density of the material also define the amount of heat that can be stored within the material, also specified as specific heat capacity. The value of specific heat determines the amount of heat that is required to raise the temperature of the material by 1K [33]**.** The specific heat is frequently expressed in the form of thermal heat capacity that can be calculated by multiplying specific heat and density [35]. The value of the specific heat capacity of insulation materials is varying with temperature; however, the moisture content has a considerable impact on the material [36]. The moisture can spread inside of the insulation material when exposed to various forms of water, such as water vapour, liquid water, or snow. The air that is present inside the cavity always contains water vapour that can be transmitted to the insulation material [19]. Regardless of the insulation material, any type of moisture can increase the thermal conductivity of the material, since the thermal conductivity of water is approximately 20 times higher compared to stationary air [33].

For comparison of various insulation materials and their thermal performances, the evaluation of thermal transmittance or U - value is required. The thermal transmittance estimates the heat flow through an insulation material and is expressed in the units of W/m^2K. The thermal transmittance is reciprocal to the thermal resistance R, which is dependent on the thickness and thermal conductivity of a material [33,37]. Consequently, in case two different insulation materials would be used on the façade, their thicknesses might need to be different to ensure the same thermal performance [38]. The range of U-values can also be

defined by prescriptive guidance. An example is the Approved Document L2B, which is applicable in England and considers the conservation of fuel as well as power in already existing buildings. Based on the document, the insulation materials that are exposed to the air cavity are required to have the U-values of insulation better than 0.7 W/m^2K. In case the insulation material does not meet the requirement, it needs to be replaced, and the improved U-value should be at least 0.55W/m^2K if this is technically, functionally, and economically feasible [39].

The thermal performance of the insulation is an important parameter, although the choice of the insulation material is influenced by a holistic approach that considers additional parameters, in particular, environmental impact, water permeability, and fire behaviour [37]. Based on the Euroclass system, the expanded and extruded polystyrene are frequently used organic polymeric materials that are classified in the range of E – F [4]. The combustible polystyrene represents a significant fire hazard for the façade system and cannot be applied on the façade due to the strengthen guidelines regarding the combustible materials on the façade system [6,40]. On the other hand**,** phenolic foam and polyisocyanurate (PIR) belong among organic polymeric materials that have an improved fire performance [30,41]. The PIR can be classified in the range of C - D, while phenolic foam is defined as C- s1, d0 [4]. In case the phenolic foam is exposed to the fire, formaldehyde is released, and the residue in the form of charcoal can continue to burn for an extended period of time [30]. The stone wool by itself represents around 35% of the European market since one of the benefits of the inorganic fibrous material is that it can be used at high temperatures ranging up to 600°C or 1000°C. The material is classified by the Euroclass system as A1 – A2 that has either no contribution or no significant contribution to the fire growth [4,24,42]. However, the thermal performance of stone wool can be affected by water due to its high water permeability [20].

The Water-Resistive Barrier can be installed in the façade system to prevent moisture damage on the insulation by the water that penetrated through the external cladding panels [43]. The WRB mitigates the inflow of water from the cavity; however, it also permits the outflow of moisture from the insulation material [44]. The WRB is generally installed over the insulation layer. The WRB can be applied in various forms; however, the most frequently used are the fluid-applied membrane, which dries into a rubber-like polymer cover, a building wrap that is mechanically attached to the insulation or a self-adhering membrane [20]**.** The WRB products are combustible, even though, based on the literature [12,45] , the fire behaviour of certain external cladding panels had a more significant effect on the performance of the façade system than the water-resistive barrier [12,45].

1.4 Variety of external cladding panels

There are various material options for external cladding panels in the rainscreen façade system, such as Aluminium Composite Material (ACM), High-Pressure Laminate (HPL), and Fibre Cement Boards [46]. Aluminium composite materials (ACM's) are frequently used cladding materials in the building industry due to their lower costs and broader availability. For this reason, they are currently representing approximately 25% of the cladding market in the USA and Europe [47]. Aluminium Composite Material, also defined as a Metal Composite Cladding (MCM), is composed of two aluminium sheets with a core in the middle [12]. However, different types of ACM can perform on various levels since the core material determines the combustibility of the cladding material [8,27]. The core material of ACM is frequently polyethylene (PE) with mineral filler, and by increasing the ratio of mineral filling, the fire performance of the ACM improves [12]. High-Pressure Laminate is comprised of layers of phenolic resin treated paper that might have added fire retardants to increase the fire resistance of the panels [12,48,49]. The fire performance of HPL is varying based on the thickness of the panels and the containment of fire-retardant chemicals. The HPL can be classified based on the Euroclass system between class B-s1,d0 that contains fire retardants, decreasing to class D for the panels that do not contain any fire retardants [48]. The application of Fibre Cement Boards as external cladding panels is increasing due to their durability, incombustibility, and moisture resistance [50,51]. The Fibre Cement Boards are classified as an innovative product since they are partially made from recycled materials [50]. For this reason, the application of Fibre Cement Boards on façade systems is increasing for the last few years, especially in Australia [51].

The fire behaviour of the façade system depends on the overall performance of the whole system rather than individual components. Accordingly, even when the applied materials have low combustibility, their combination would need to be tested to verify the fire behaviour of the façade system [21,47].

1.5 European evaluation of façade systems

In Europe, there are currently 12 different tests that are used for the evaluation of façade systems that range from full-scale to small-scale tests [52,53]. The testing configuration depends on the executed façade test and can vary between a single wall and a corner configuration [52]. Depending on the test, the façade system can either be evaluated for the fire that occurs outside the building façade or for the internal building fire with flames emerging through an opening. The façade system can also be assessed for the flame spread along the external cladding panels or the flame spread inside the air cavity. Some of the tests also have additional requirements regarding the amount of falling debris off the façade

system during the tests, since it could potentially start a secondary fire or jeopardize the rescue services [1].

The severity of experimental tests is specified in terms of the imposed heat flux on the façade and can differ between the tests from as low as 40 kW/m^2 to 110 kW/m^2. Based on the literature about post-flashover fires, the realistic values of heat fluxes vary between 70 - 80 kW/m^2 to approximately 100 kW/m^2 for a single wall experiment. For corner façade tests, the heat flux values will be higher than for a single wall experiment because there will be less air entrainment and higher radiation view factors that will increase the heat flux value [45].

A full-scale test that is used in Sweden for evaluating façades is SP Fire 105, while a full-scale test BS 8414 is more applied in Great Britain [53]. The standardized test ISO 13785 has a full-scale test and an intermediate-scale test. The full-scale test ISO 13785-2 is used in Slovakia, while the intermediate-scale test ISO 13785-1 is more applied in the Czech Republic [52]. Both of the ISO 13785 tests evaluate the façade system for a post-flashover scenario, with the fire origin inside of the building and flames emerging through the window opening on the façade [6,20]. The execution of full-scale tests is expensive and time-consuming; for this reason, intermediate-scale tests are proposed to enable testing the influence of different façade components as well as different system configurations. In this way, the intermediate-scale tests will extend the scope of the full-scale tests [47]. Tests BS 8414-1 and ISO 13785-2 are considered to represent an acceptable representation of fire impingement into the façade system [54]. The problems that could occur with intermediate tests due to the reduced scale include insufficient or incorrectly scaled down thermal exposure [9]. The intermediate-scale test ISO 13785-1 is a screening test of ISO 13785-2 and has the experimental set-up similar to the one-third scale of the BS 8414-1 test [9,55]. The intermediate-scale experiments that were performed on wooden façades also showed a correlation with the full-scale tests, based on the heat flux measurements and flame spread times [56]. As previously mentioned, the façade tests vary depending on the country. For this reason, the European harmonised approach for assessment of the façade systems is currently under development that will be based on BS 8414 and an intermediate-scale test DIN 4102-20 [1]. The ISO 13785-1 and the DIN 4102-20 both consider the fire scenario, where the fire emerges through the window opening into the façade. However, DIN 4102-20 is mostly used in Germany and Switzerland and exposes the façade to approximately 60 kW/m^2 [45,52].

The small-scale experiments such as cone calorimeter tests are usually only applied for testing of individual components in a façade system since the materials are only exposed to specific fire exposure. Currently, there is no practical method with which small-scale experiments would predict a fire performance of full-scale experiments. Small-scale experiments might be able to predict the fire behaviour of individual components in full-scale experiments; however, additional tests would be required [12].

1.6 Objectives

The objective of this thesis is to estimate the fire behaviour of three intermediate-scale façade tests that represent well-ventilated façade systems by varying their material compositions and assessing their performance by measuring the heat release rate. The results of the intermediate-scale experiments will be compared to formerly executed intermediate-scale tests, to provide additional information regarding the influence of external cladding panels, type of insulation, cavity width as well as cavity barriers on the heat release rate. This thesis will also provide additional insight regarding the correlation between the intermediate-scale tests and the cone calorimeter data by testing identical materials on both scales.

1.7 Overall methodology

The experiments will be composed of eleven cone tests and three intermediate-scale façade tests. The inorganic polymeric material that will be tested in the cone calorimeter will be represented by stone wool. However, due to the high-water permeability of stone wool, the cone tests will be repeated by testing the composite of stone wool and WRB. On the other hand, the organic polymeric insulation material that will be examined is phenolic foam. The materials that will be initially tested at the cone calorimeter will afterwards be examined on a larger scale as part of the intermediate-scale façade system. The façade systems that are going to be tested include the calcium silicate boards as the external cladding panels, while the insulation material will vary between the experiments as in cone calorimeter.

1.8 Limitations

The façade systems are currently being evaluated in Europe with 12 different tests, that have distinctive test configuration and instrumentation. The experimental part of the thesis will be performed by executing intermediate-scale tests following the standard ISO 13785-1 that is mainly used in the Czech Republic and exposes the façade to an approximately 50 kW/m^2. Even though several studies on post-flashover fires revealed that the heat fluxes of approximately 70-80 kW/m^2 are more representative values of reality [45].

The limitation of the experimental part is that by following the standard ISO 13785-1, the defined fire scenario is the fire that develops inside of a building and emerges through the window opening and spreads along the façade. However, other fire scenarios that might also commence the façade fire are not in the scope of this thesis [1].

Even though the intermediate-scale experiments on wooden façades showed a correlation with the full-scale façade tests, they may still not be able to estimate the fire behaviour of a full-scale façade test [56]. For this reason, the full-scale experiment would still need to be conducted, even though the ISO 13755-1 is a screening test of ISO 13785-2.

The restraint of the experimental part is the lack of repeatability of each tested configuration in the cone calorimeter as well as in the intermediate-scale tests. There is also a lack of the reproducibility of the environmental conditions present in the laboratory [6,57].

The tested façade systems will not be protected with cavity barriers against the vertical flame spread within the air cavity, due to different regulations among the countries and for the better observation of the flame spread within the air cavity [12].

This thesis will only consider the rainscreen cladding system, which represents a well-ventilated façade system [3,12].

2. Literature review

2.1 Assessment of the façade performance

The fire development is frequently expressed as the heat release rate or energy release rate, which usually changes in time and quantifies the fire size, its rate of fire growth, and determines the fire hazard [56,58,59]. The experiments that were conducted by Agarwal, Wang, and Dorofeev [45] demonstrated that the fire performance of the overall façade system could be assessed by the heat release rate through the oxygen consumption calorimetry, which is further described in Chapter 5.1 [45,56]. The experiments were composed of two parallel panels while imposing a heat flux above 100kW/ m^2 onto the façade and following the ANSI/FM 4880 standard. The external cladding panels of tested set-ups included different types of ACM. The results demonstrated that the tested external cladding panels have the highest contribution to the heat release rate, while the insulation and the WRB have a minor influence. It was estimated that 1.8 mm thick WRB in the form of a fluid-applied membrane contributes approximately 250 kW when tested with the external cladding panels of ACM with the fire-retardant core defined as ACM-FR [45].

In a similar manner, the experimental data that was based on the intermediate-scale tests ISO 13785-1 also demonstrated that external cladding panels of ACM have the most significant effect on the heat release rate. The experiments were executed at 50 mm cavity width and were composed of nine tests, including three different types of ACM with each of them being tested with phenolic foam, stone wool, and PIR. The external cladding panels varied from ACM-PE, which included a core material of polyethylene, ACM-FR, including the 70% of non-combustible mineral to ACM-A2 with 90% of non-combustible mineral fill. The tests with ACM-FR and ACM-A2 demonstrated a similar maximum heat release rate pattern that was below 300 kW with all three types of insulation. On the other hand, the tests conducted with ACM-PE showed a maximum heat release rate of around 5MW. The smallest contribution to the fire development had the ACM-A2 with stone wool, which was closely followed by the ACM-A2 tested with the phenolic foam as well as ACM-FR with stone wool. Based on the total heat release rates of PIR and phenolic foam with various types of external cladding panels, it was demonstrated that the PIR releases approximately 5% more energy than phenolic foam [47,55].

Burning in a cavity is defined by the chimney effect as well as by the limited air supply for the combustion process [21]. The chimney effect indicates the pressure differences within the cavity that occur due to the temperature differences between the flue gases and the outside air. However, the draft that is created by the chimney effect is not only dependent on the temperature differences but also the height of the cavity [60]. Choi & Taylor [61] conducted the experiments at the 5 m high vertical rectangular duct that was lined with glass wool

insulation. The experiments were conducted at different cavity widths and demonstrated that the critical cavity width is 25 mm. The oxygen supply within the cavity that is smaller than 25 mm is not adequate to support the combustion process of the insulation material. The experiments that were conducted at the cavity width of 25 mm and 38 mm also showed that the fire propagation within the façade system in both cases increased, even though the applied insulation had a low contribution to the fire development [61].

2.2 Heat transfer modes

In the case of a fire, the thermal energy is accounted for the material behaviour during the fire; the flame spread as well as the fire growth [21,62]. Thermal radiation, thermal convection, and thermal conduction are the three heat transfer modes that transport the thermal energy within the fire [21]. The heat can be transferred with conduction or convection purely through a medium that can be represented in the form of gas, liquid, or solid [63]**.** Conduction and convection are both present in fluids; however, conduction in fluids is comparably smaller than in solid materials [21]. The main difference that can be identified between convection and conduction is correlated to the ordered flow or bulk motion of the medium [63]. The convection is defined as the heat transfer mode that contains the bulk movement of molecules within the fluid, and it can often be identified between the fluid and solid. Convection is present when the fluid is in motion near the solid, and the energy can be transferred to the surface of the solid material when there is a temperature difference between the mediums. The energy is transported from the fluid to the solid material through conduction and radiation. The conduction is correlated to the temperature distribution in the solid that is dependent on the thermal conductivity of the material, specific heat, and density [21]. In the solid material, the energy is always diffused from the region with a higher temperature to the part of the solid material with lower temperatures [21,63]. All three heat transfer modes require a temperature difference to transfer the energy; however, the energy is transmitted by radiation through electromagnetic waves; therefore, the medium is not required [63]. Each object that has the temperature above 0 K transmits the energy in the form of radiation that can be transferred between two objects at a certain distance from each other [63].

The thermal radiation is significant, primarily due to the energy that is transferred from flames and from the heated objects to the solid material, which can be quantified in the form of radiation heat flux [21]. An energy balance of heated solid material, while exposed to the radiant heat source, can be observed in Figure 4**.** The radiation is defined as $q''_{rad,inc}$ and convection q''_{conv} are the heat transfer mechanisms that are transferring the energy to the surface of the solid material; however heat transfer in the form of conduction q''_{cond} is transferring the energy through the thickness δ of the material [64]. On the other hand, the

material does not only receive the energy, but a portion of it is also reflected from the surface in the form of radiation q''_{rad} [21,65].

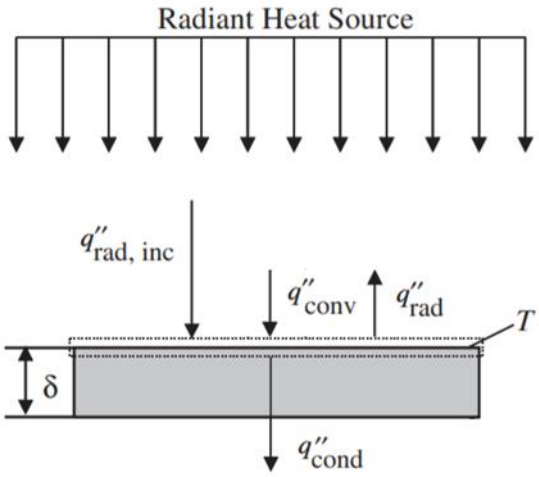

***Figure 4**: Energy balance at the surface of a solid material modified from [65]*

The façade system involves all three heat transfers, with radiation being present in the flame, while convection and conduction are heating the air in the cavity ahead of the flame. The heat transfer in the form of conduction is present inside of the solid materials [64]. The external cladding panels and the insulation material are within a façade system only separated by the cavity width that does not only limit the oxygen availability but also increases the flame spread due to the radiation feedback from both façade elements [21].

2.3 The heat flux and flame height measurements

During the fire testing, the total heat flux gauges are installed within a façade, which measures the combined effect of radiation as well as convection [65]. Foley & Drysdale [66] carried out the experiments that were composed of two parallel panels, while varying different parameters, such as the burner location, airflow conditions, and the cavity width. The experiments showed that the heat flux values increased by reducing the distance between the panels [21,66]. Ris & Orloss [66] also conducted experiments with the two parallel walls; however, the tests included a range of fuels that burned in between the panels. The results showed that the heat flux values from the flames are dependent on the sootiness of fuels [21,66]. The heat flux values also vary throughout the height of the façade system, therefore the burner that is positioned on the ground influences the measured values of heat fluxes. The lower the distance between the burner and the heat flux gauge, the higher the measured heat flux [67].

Experiments that consisted of varying the cavity width from 200 mm to 100 mm between two parallel incombustible panels, while modifying the mass flow of the propane gas burner also demonstrated increased heat flux values along with the height of the test sample. The heat flux values increased primarily when either the cavity width was reduced or the mass flow was raised, consequently increasing the heat release rate [57]. The reduction of the cavity width also influenced the flame height within the cavity. The flames extend through the entire cavity by reducing the cavity width to 40 or 30 mm, depending on the mass flow from the burner [57].

However, the mass flow is not only dependent on the burner, but it can also vary with the experimental set-up, as confirmed by Ingason. He performed multiple experiments in two-dimensional rack storages by simultaneously varying the distance between the horizontal and vertical flues as be observed in Figure 5. The results demonstrated that the influence of the horizontal flue heights on the vertical flue flow is negligible. However, the increase of the vertical flue distance leads to the linear rise of the mass flow rate [68].

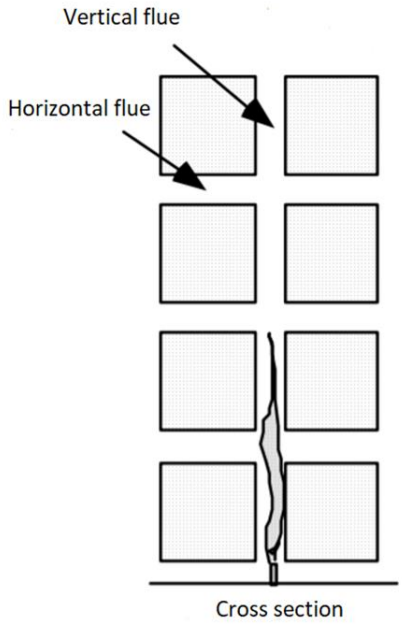

***Figure 5**: The schematic representation of horizontal and vertical flues modified from [68]*

2.4 Burning of the solid material

During the fire, the heat is transported ahead of the flame to the unburned part of the solid fuel to increase its temperature. The transferred heat does not only increase the temperature of the solid fuel but also causes its vaporization. The process that causes the transition of the solid material to the gas phase is defined as pyrolysis and usually indicates the breakdown of molecules to smaller molecules. The produced fuel gases during the vaporization are mixed with the air in the vicinity of the solid that leads to the combustion of the gases and the

development of the sustained flame [63,64,69]. The energy that is released during the combustion process is transported ahead of the flame to the unburned part of the solid material; therefore, the energy cycle is attained for the flame spread process [64]. However, the ignition of the material can only be achieved in case the material is exposed to the heat flux that is above its critical level, also defined as the critical heat flux [63].

Exposure of the material to the different heat transfer mechanisms will not only cause the "onset of pyrolysis," but the material will also begin to degrade and thermally decompose that could potentially lead to the loss of its functionality. Some of the materials might melt, shrink, scorch or start charring during the heating that could have an influence on their mechanical as well as thermal behaviour [21,70]. For this reason, the materials that are implemented in the façade system, especially as part of the external cladding panels, have an influence on the fire performance of the entire system. The external cladding panels are quite thin, and in case of a flame spread within the cavity, the panels are more prone to ignition. Therefore, the material that has a low melting temperature, composing the external cladding panels, could increase the cavity width of the façade system [21].

2.5 Methods for assessing material degradation

The processes that occur within the materials while exposed to heating can be assessed through microscale experiments that only analyse a few milligrams of materials. The microscale experiments can be conducted with the thermogravimetric analysis (TGA) as well as the microscale combustion calorimetry (MCC). The TGA measures the mass loss rate as a function of time, while the MCC provides information about the heat release during the combustion process [8,71]. Both methods are providing additional information regarding the pyrolysis reaction; however, neither of them obtain the temperature at which the gas products ignite [21]. For this reason, the flammability properties of the material are frequently evaluated through a bench-scale testing apparatus defined as the cone calorimeter, which is based on the principle of oxygen consumption during the combustion process, that is, further described in Chapter 5.1 [8,71].

3. Insulation materials

The properties of the insulation materials can be divided into various groups, such as physical characteristics, environmental influence, and properties that are more correlated to public health. The physical characteristics include the density of the insulation material, sound absorption, mechanical strength as well as moisture and fire resistance. The environmental influence of the insulation materials includes the gas emissions that are produced during the manufacturing process, their reusability, and the potential for recycling. The third group of

properties considers the effect of insulation materials on public health during their entire life cycle that includes their production, application on buildings, and disposal [72]. However, within the group of physical characteristics also thermal properties of insulation can be defined, which determine the heat transfer through a material. Thermal properties of insulation generally include density, thermal conductivity, specific heat, as well as thermal expansion coefficients [73]. The product of thermal conductivity, density, and specific heat is defined as thermal inertia that characterizes the rate at which the surface temperature rises in a specific material and consequently also determines the time to ignition [63]. The surface temperature of materials with lower values of thermal inertia will increase quicker than of materials with higher values when exposed to identical heat flux values [74,75]. The purpose of this thesis is to evaluate the fire behaviour of various façade systems, and for this reason, the thermal properties of phenolic foam and stone wool will be discussed further.

3.1 Phenolic foam

The phenolic foam is a brittle material with low strength capabilities that prevent the material from being widely used during the construction process. However, the material has good corrosion resistance, thermal properties as well as fire-resistant capabilities, therefore it is a suitable insulation material [30,40,76]. Thermal properties of the phenolic foam are correlated to its structure, which contains a high ratio of closed cells that are filled with an insulating blowing agent [30]. During the phenolic foaming process, which includes a resol resin alongside acid catalysts, surfactants and blowing agents, the temperature should be either below 100°C or the entire process should be performed under pressure. In case the temperature would be above 100°C, the water inside of the foam would start evaporating, consequently increasing the pressure that might cause the cells within the foam to rupture and therefore reduce the thermal properties of the material [30,77]. The thermal characteristics of phenolic foam are comprised of low thermal conductivity that varies between 0.018 – 0.028 W/mK and is correlated to the distribution of the cells and their content [33,37]. Even when the value of the thermal conductivity is in the upper part of the range, the value is still below 0.03 kW/mK; therefore, the material has excellent thermal performance [33]. The density of the phenolic foam can range up to 160 kg/m^3 and has a significant effect especially on the physical properties of the material such as its mechanical strength and the moisture absorption [37,78–80]. The phenolic foam also has a specific heat capacity that is frequently in the range of 1.3-1.4 kJ/kgK [37,81].

In the European market, the manufacturers of phenolic foam place the protective layer in the form of a foil on the surface of the material. However, in the literature [70] the experiments that were conducted with the phenolic foam in the cone calorimeter did not involve the protective layer to provide only the additional information regarding the core and not the overall composite. This needs to be considered in the analysis of the results since the

protective layer due to its low emissivity would contribute to the values of the results. The cone experiments were conducted with the phenolic foam that had the thermal conductivity in the range of 0.021- 0.024 W/mK, the density of 38 kg/m^3 as well as the specific heat capacity of 1.5 kJ/kgK demonstrated, that the critical heat flux for phenolic foam is at 22 kW/m^2. The main visual observations during the tests indicated that the phenolic foam begins to char, which is followed by its ignition when the heat flux passes the critical heat flux value. However, the rate of the char residue on the surface of the material is also dependent on the external heat flux. The pyrolysis of the solid material becomes significant at the “critical temperature," which was found to be during experiments for the phenolic foam at 425°C [70].

During additional experiments that were executed with the same type of phenolic foam, it was observed that while heating the phenolic foam began to crack and spall, which confirmed a brittle behaviour of phenolic foam. In the experiments, it was also estimated that the peak heat release rate per unit area was in the range of approximately 25 to 100 kW/m^2 [41]. The experiments that were carried out with three different types of phenolic foam at the heat flux of 50 kW/m^2 had a maximum heat release rate in the range of 62 to 64.8 kW/m^2. The phenolic foams were tested without the external aluminium foil facing and had the density in the range of 41.8 kg/m^3 to 45.0 kg/m^3 [46].

3.2 Stone wool

Stone wool can also be referred to as rock wool and is used in industry, transportation as well as in construction due to its thermal insulation properties, sound impedance, and fire resistance [30,82,83]. The material has a porous structure with solid fibres that are containing voids in between [84]. Stone wool is produced at the temperature of 1600°C by melting a combination of rocks that involves dolerite, basalt, and diabase [37,83,85]. The melted mixture is bonded together by organic binders and water-repellent oils [37,84]. However, due to the growing environmental awareness, there is an opportunity of substituting the natural materials within the stone wool by using an industrial waste material that would otherwise stay in the landfill [83]. The thermal characteristics of stone wool include thermal conductivity that varies between 0.033 and 0.04 W/mK, the density of approximately 40-200 kg/m^3 as well as specific heat that ranges from 0.8 to 1.0 kJ/kgK [37]. Range of thermal conductivity classifies the stone wool as the insulation material that has the thermal performance of most insulation materials as previously defined in Chapter 1.3 [33].

The stone wool is exposed to heating that can generate a certain amount of heat due to the burning of organic binders and oils within the stone wool, which usually begins at approximately 200°C. For this reason, the temperature inside of the stone wool might even increase locally above the temperature in the surroundings [21,73,84]. The experiments that were conducted with MCC and TGA demonstrated two different reactions occurring within the stone wool while heating. At temperature between 200°C and 600°C the reactions

correlated to the pyrolysis and oxidation of the organic binders; however, the temperature that is above 700°C corresponded to the crystallization of the fibres [86].

In Figure 6**,** a correlation between the thermal conductivity and density at ambient temperature can be observed. On the left-hand side is presented a thermal conductivity as a function of density, depending on the orientation of the fibres within the stone wool with k_V representing the vertical orientation of the fibres, while k_H defining the horizontal fibres. The orientation of the fibres is especially crucial at the densities around 100 kg/m^3, where the difference of thermal conductivity can be even of 33% for horizontally oriented fibres compared to vertical fibres. On the right-hand side of Figure 6 can be seen the contribution of the three heat transfer modes to the total thermal conductivity. With the exposure of the stone wool to a high temperature, the density will begin to decrease due to the thermal decomposition of the binders. However, as can be seen in Figure 6**,** the thermal conductivity will increase for the densities in the range of 20 – 100 kg/m^3, and the radiation will become a dominant heat transfer mode [87].

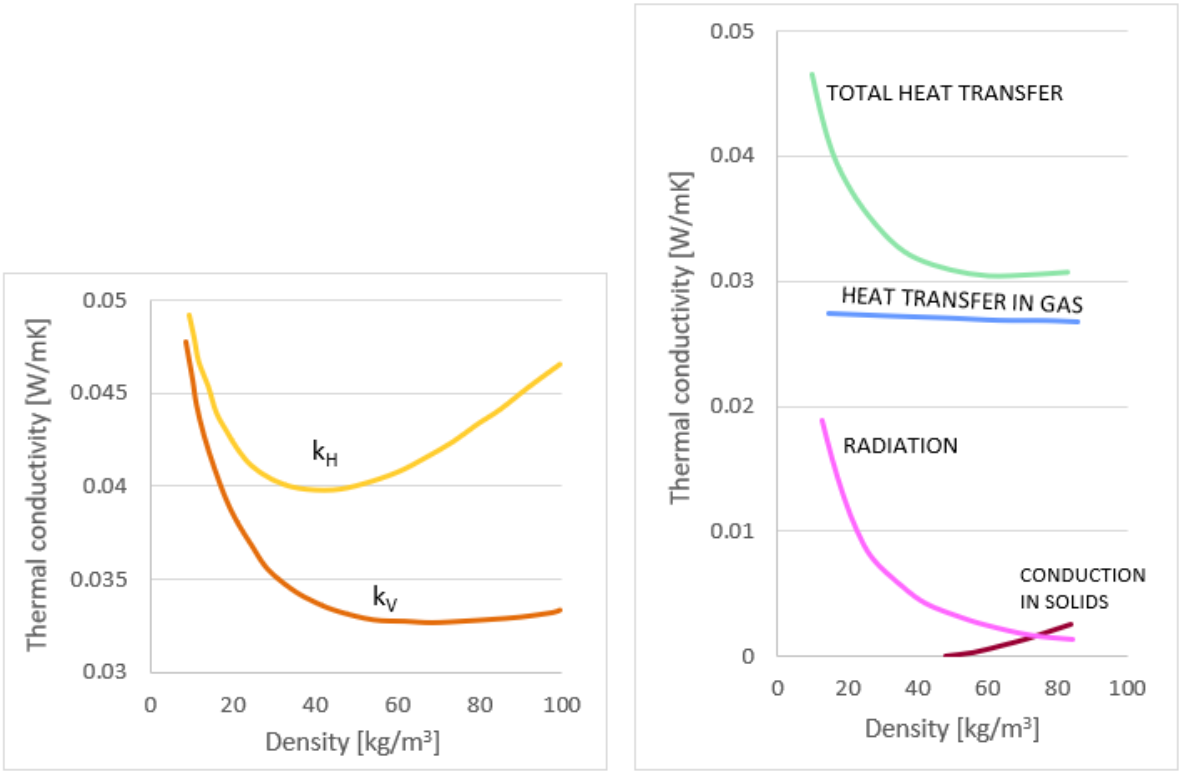

***Figure 6**: Thermal conductivity as a function of density redrawn from [87]*

In the literature [70], the experiments that were conducted in the cone calorimeter by exposing the stone wool to the heat flux values up to 88 kW/m^2 demonstrated that the material did not ignite. The tested stone wool had the thermal conductivity in the range of 0.034 to 0.044 W/mK, the density of 40 kg/m^3, and the specific heat capacity of 0.84 kJ/kgK. The tests indicated that the critical temperature is not applicable for the material; however, the maximum heat release rate was not defined [70]. On the other hand, the experiments

that were carried out at the heat flux of 50 kW/m^2 with the stone wool that had the density of 37 kg/m^3, the maximum heat release rate that was defined at 5.6 kW/m^2 [46].

As already mentioned, the moisture present within the material affects the thermal conductivity of the material. In the literature [19], two different types of stone wools were tested for several days to assess their absorption of water due to the porous structure of the material. The tested materials are defined as low and high-density stone wool, as presented in Table 2 [19].

***Table 2**: Material properties of various types of stone wool [19]*

Material: stone wool	Density [kg/m^3]	Thermal conductivity [W/mK]
Low density	30	0.036
High density	94	0.035

Both types of stone wool were exposed to capillary water for several days that can occur when the material is directly in contact with the ground [19]. The results are presented in Figure 7, and as it can be observed, the differences between the two different densities of stone wool are not significantly different from each other. However, the stone wool with high density is after several days more prone to the absorption of capillary water than low-density material.

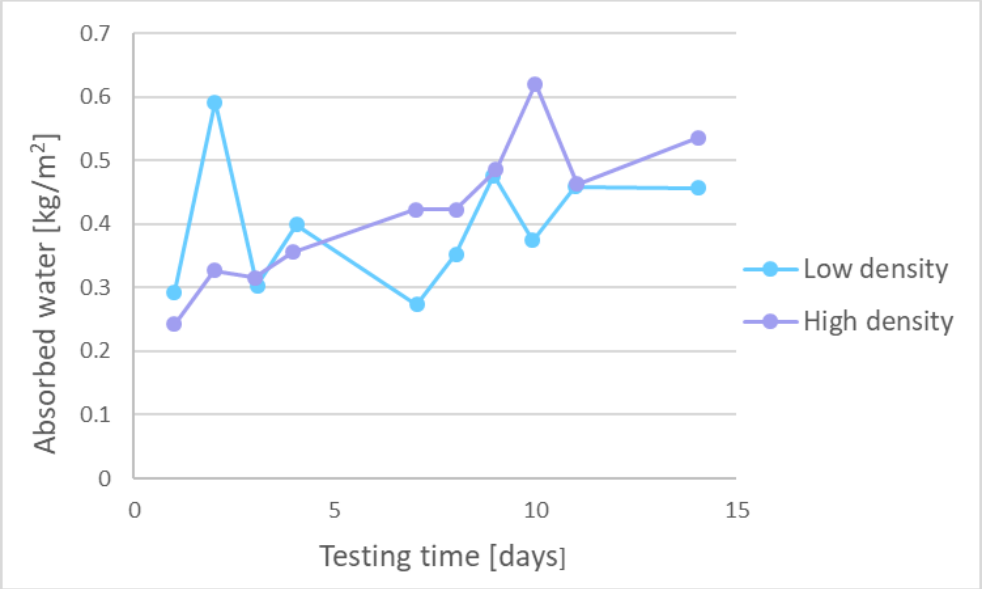

***Figure 7**: Capillary absorption of water by stone wool redrawn from [19]*

The samples of the stone wools were also tested for the water absorption by diffusion. The partial pressure of the water vapour within the structure is usually higher than the partial pressure of the exterior water vapour; therefore, air moisture is transferred by diffusion to the external wall of the structure, which has the applied insulation. The stone wool samples were tested for several days, and the results are presented in Figure 8 [19]. As it can be

observed, the high-density stone wool absorbs after 25 days approximately 10 kg/m^2 than low-density stone wool.

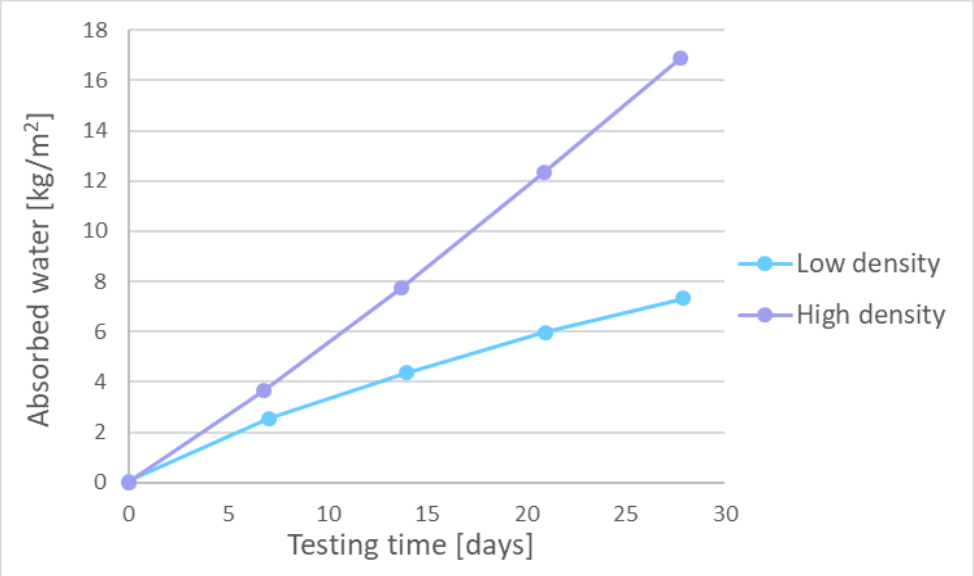

***Figure 8**: Water absorption by diffusion redrawn from [19]*

During the last few years, there has been a significant amount of attention on the moisture accumulation in building materials, especially during the construction process, when the materials can be exposed to the rain for an extended period of time. As a protection of the building materials, especially during the construction, when the façades are still partially open systems, a WRB can be installed to protect the insulation material. However, the WRB can also be implemented in fully built façade systems to protect the insulation from the water that penetrates through the external cladding panels [19,43,88].

4. Water resistive barrier

There are various types of water-resistive barriers that are available on the market; however, the focus will only be on the water-resistive barrier in the form of the self-adhering membrane that will also be tested in the intermediate-scale tests and cone calorimeter. The tested WRB is composed of two layers of thermoplastic elastomers, covered with acrylic coating [88].

As described by Amin and Amin [89], the thermoplastic elastomers (TPE) are a versatile physically cross-linked polymers that are composed of two different polymers that can be defined as plastic and rubber. The TPE is produced by the physical mixing of the thermoplastic and elastomer that does not involve any chemical bonding between the polymers; therefore, the material properties are a combination of the two polymers. For this reason, the TPE is a two-phase material because each of the molecules within the material has the elastomeric part and the restraining physical cross-linking part [89].

In Figure 9, the modulus of elasticity as a function of temperature for TPE is presented, and as it can be observed, the material has a range of temperatures that define the “useful state." TPE properties of elastomer and thermoplastic are in the "useful state" in the form of rubber. In case the temperatures that can either be defined as T_g or T_m are below the lower boundary line, both of the TPE properties transition to their brittle state. On the other hand, in case the temperatures T_g or T_m increase beyond the "useful state," the material will transform into mouldable liquid [89]. The WRB that will be tested has the temperature range of the “useful state” between -50°C and 100°C [88].

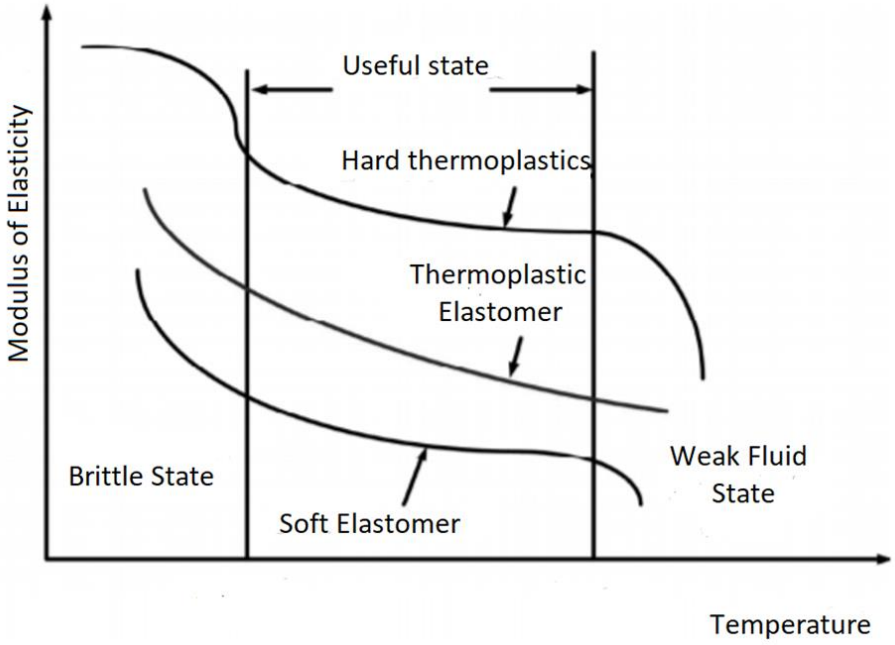

***Figure 9**: Modulus of elasticity as a function of temperature for TPE modified from [89]*

5. Methodology

5.1 Oxygen consumption calorimetry

The oxygen consumption calorimetry has first been identified in 1917 by Thornton, who demonstrated that the heat of combustion per unit of consumed oxygen is almost identical for a vast majority of fuels. Huggett afterwards discovered that most liquids, gases, and solids release almost a constant amount of energy that was defined as 13.1 MJ/kg of consumed oxygen [58,63]. Since then, the method has been refined during 1970-1980 and became widely applicable for estimating the heat release rates. The oxygen consumption calorimetry is a universally accepted method that can be applied either to small-scale or full-scale experiments [59,63]. In this master’s thesis, the method of oxygen consumption calorimetry

has been applied for intermediate-scale experiments as well as for the small-scale experiments that were conducted with the cone calorimeter.

As described in the SFPE Handbook of Fire Protection Engineering**,** the method is based on the requirement that all the combustion products from the experimental test are collected and removed through an exhaust duct that is located at a distance that enables adequate mixing of gases [63]. In the exhaust duct, the flow rate and the gas composition is measured, specifically the O_2 concentrations, however for increasing the accuracy, the CO_2, CO, and H_2O can also be measured [56,63]. The schematic representation of the oxygen calorimeter methodology for intermediate or full-scale experiments is presented in Figure 10.

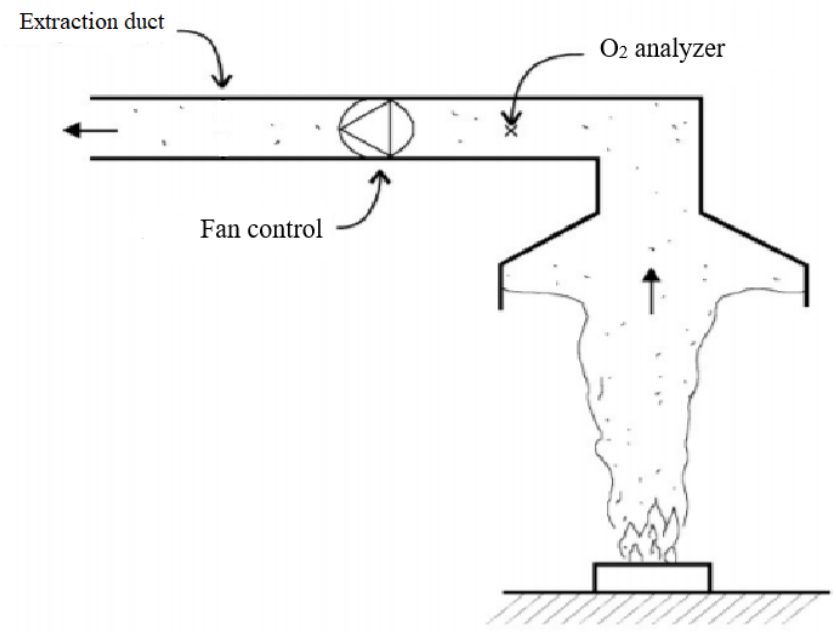

Figure 10*: Schematic representation of oxygen consumption calorimetry for intermediate or full-scale experiments modified from [90]*

The simplification that is assumed is that the incoming gas inside of the hood contains only O_2, CO_2, CO, H_2O, and N_2 [56]. The combustion products that are extracted through the hood and proceed through the exhaust duct are initially dried to remove the water vapour from the gas before executing the gas analysis [56,63]. The heat release rate is calculated with the following equation [91]:

$$\dot{q}\,(t) = \left(\Delta h_{hc/ro}\right)(1{,}10)C\,\sqrt{\frac{\Delta p}{T_e}} * \frac{X_{O_2}^0 - X_{O_2}}{1{,}105 - 1{,}5X_{O_2}} \quad (1)$$

The simplification that is accounted for during calculations, that the energy released during complete combustion is constant at 13.1 MJ/kg of consumed oxygen [56,63]. Therefore, the $\Delta h_{hc/ro}$ was assumed to be constant at 13.1 MJ/kg. In equation 1, the C represents the orifice flow meter calibration constant, which is defined at 0.03759, while Δp represents the orifice

meter pressure differential. The initial value of oxygen analyser reading is specified as $X_{O_2}^0$ and X_{O_2} only defines the oxygen analyser reading, while T_e specifies the absolute temperature of the gas at the orifice meter [91].

5.1.1 Cone calorimeter

The cone calorimeter was used to determine the fire performance of different materials. The main components of the apparatus are the cone heater, spark igniter, and the load cell, as can be observed in Figure 11. The experiments in the cone calorimeter can either be performed with the cone heater in a horizontal or vertical orientation. During the tests, the cone heater was positioned in a horizontal orientation with the spark igniter located over the centre of the horizontally located sample. By moving the spark igniter closer to the surface, due to the higher amount of flammable mixture, there is a higher probability of ignition than at a distance higher from the sample [63]. The heat release rate based on the oxygen depletion calorimetry was calculated during the experiments with equation 1.

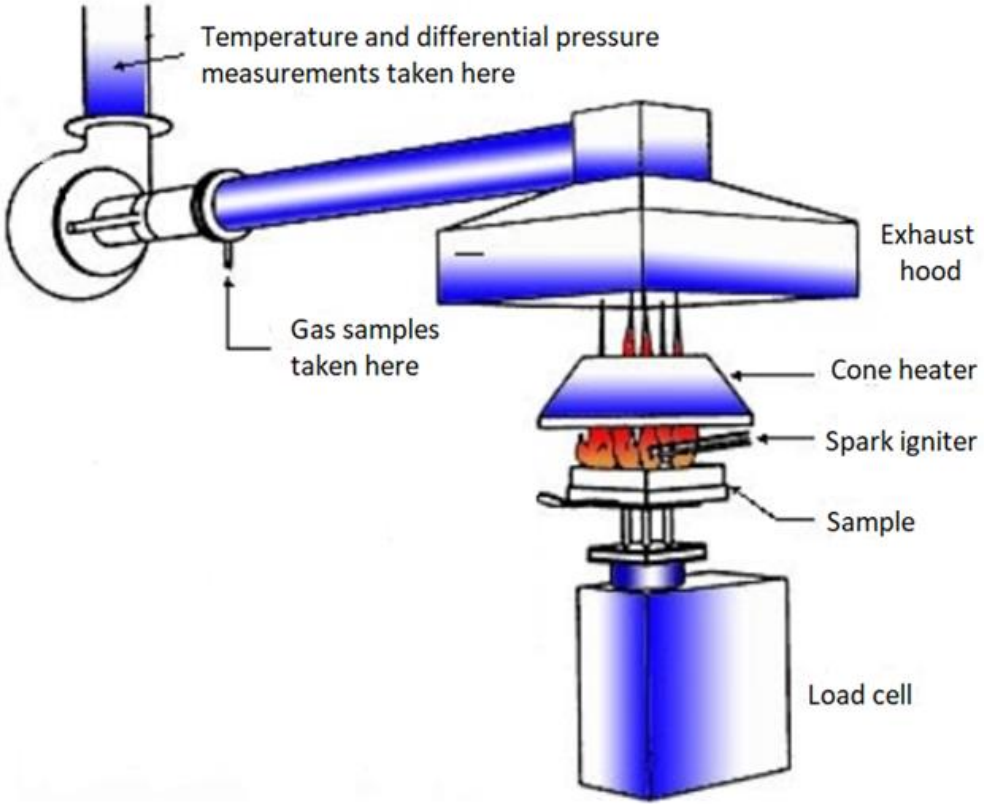

***Figure 11**: Composition of the cone calorimeter modified from [92]*

The cone heater exposes the sample to the external radiation, which represents an evolving fire; however, it cannot define a real fire scenario since the materials are usually not ignited by a spark igniter and exposed to the radiation from above [93].

In the cone calorimeter is usually measured time to ignition t_{ig} of the material at different heat fluxes, from which it can be determined the surface temperature at ignition and thermal inertia of the material [94,95]. The correlation between time to ignition and heat flux determines the temperature profile within the specimen [96]. The solid is defined as thermally thin when the temperature gradient inside of the material is negligible, while the thermally thick material has a significant temperature gradient within the solid [63]. According to the literature [96], the material can be determined to be either thermally thin or thermally thick by plotting the times to ignition in the form of $(1/t_{ig})^n$ as a function of the applied heat flux. The n value is defined for the thermally thick material at 0.55 and for the thermally thin material at 1. Based on the least-square method the correlation coefficient R^2 which is determined for both of the n values specify whether the material is thermally thick or thermally thin based on its vicinity to 1 [96].

The surface temperature at the time of ignition is dependent on the critical heat flux $\dot{q}_{cr}$", the emissivity of the material ε as well as on the convection coefficient h_c. From the linear correlation of times to ignition $(1/t_{ig})^n$ as a function of the applied heat flux, the critical heat flux is the intercept of the line with the abscissa [74]**.** The value of the emissivity is dependent on the ability of the material to emit energy and is for most building material defined above 0.8 [97]. On the other hand, the values of the convection coefficient for the horizontally oriented specimens vary in the literature from a constant value of around 10 W/m^{2}K to a function of applied heat flux. The method of determining the convection coefficient as a function of applied heat flux will be considered in the analysis of the cone calorimeter results [95]. The surface temperature at the time of the ignition can be calculated from the equation below [74]:

$$\varepsilon \dot{q}_{cr}" = h_c\,(T_{ig} - T_\infty) + \varepsilon\,\sigma\,(T_{ig}^4 - T_\infty^4) \quad (2)$$

In equation 2, the T_{ig} defines the surface temperature at ignition in [K], the ambient temperature is defined with T_∞ in [K] while, the σ represents the Stefan- Boltzmann constant with the value of 5.67 * 10^{-11} kW/K^{4}M^2 [74,96]. The calculated surface temperature can then be applied for the calculation of the total heat transfer coefficient h_{ig} with equation 3 [74]:

$$\varepsilon \dot{q}_{cr}" = h_{ig}\,(T_{ig} - T_\infty) \quad (3)$$

The total heat transfer coefficient is a required parameter for determining the thermal inertia $k\,\rho c$ with equation 4, where $\dot{q}_e$" represents the irradiance from the cone heater in [kW/m^2] [74]:

$$\dot{q}_e" = \dot{q}_{cr}" \left[1 + 0.73 \left(\frac{k\,\rho c}{h_{ig}^2\,t_{ig}}\right)^{0.55}\right] \quad (4)$$

5.2 Description of the cone calorimeter test set-up

The cone experiments were executed following the standard ISO 5660 [91] and exposing three different specimens to the heat flux of 20 – 50 kW/m^2. The heat flux values of 35 kW/m^2 and 50 kW/m^2 are frequently selected values of irradiance from the cone heater, due to their similarity to the developing fires. The heat flux values of around 50 kW/m^2 also examine the combustion properties of the material as well as its flame spread [93].

The first tested sample was stone wool, which had the Euroclass rating of A1 [98]. The stone wool and the phenolic foam were both Kingspan products. Therefore, the stone wool is also defined as K-Roc, while the phenolic foam is named K15. The thermal properties of stone wool, as well as phenolic foam, are presented together in Table 3. The K15 was not tested in the cone calorimeter, due to the lack of material. However, the K15 without the external aluminium facing was already tested in the cone calorimeter; therefore, the result was only analysed together with the additional experiments that were carried out in the cone calorimeter.

***Table 3**: Thermal properties of stone wool and phenolic foam*

Thermal properties	Stone wool	Phenolic foam
Density [kg/m^3]	45	35
Thermal conductivity [W/mK]	0.034	0.02
Specific thermal capacity [kJ/kgK]	1	1.88

The tested samples also included the WRB in the form of a foil, composed of two layers of TPE that was covered by the acrylic coating. The tested WRB had the fire performance classified as B-s1, d0, as presented in [88]. However, the thermal properties of the WRB were unknown [88]. The third tested sample was a composite that consisted of the WRB that was placed on top of the stone wool, as it can be seen in Figure 12. The tested stone wool had a thickness of 50 mm, while the WRB thickness only measured 0.5 mm and a density of 540 kg/m^{3,} which was calculated as presented in Chapter 5.3.1. For this reason, the tests that only included a WRB had ceramic wool placed underneath to overcome the difference in the thicknesses.

***Figure 12**:Sample composed of stone wool and WRB*

The tests that involved WRB had a placed wired grid on top of the material to prevent its contraction when exposed to the heat flux, following the standard ISO 5660 [91]. During the tests, the wired grid absorbed some of the heat from the cone heater that could have prolonged the ignition time of the samples [99]. In Figure 13, the stone wool sample can be observed as well as test 2, which included the WRB and the wired gird.

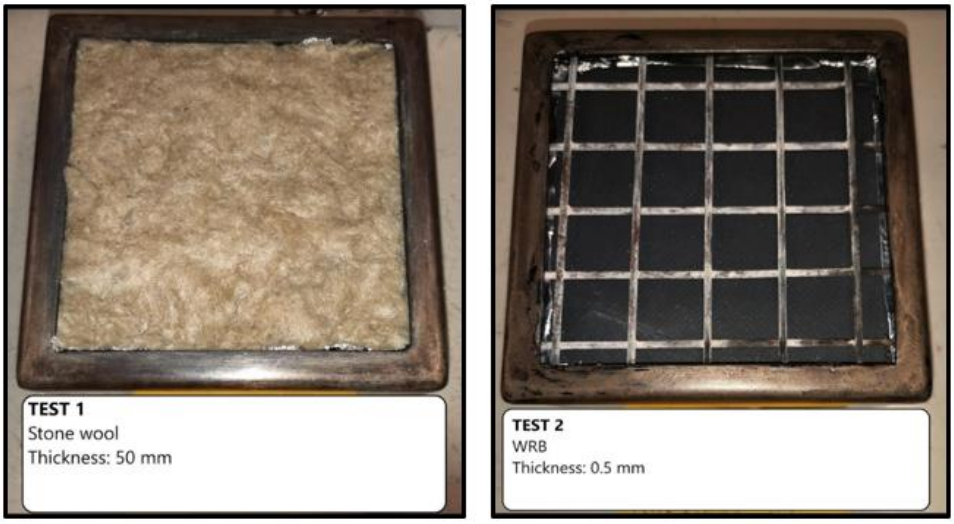

***Figure 13**: Stone wool and WRB sample*

The bottom of the cone heater is defined to be positioned 25 mm from the specimen. However, due to the thickness of the steel wires that were measured to be 3.6 mm, the sample was positioned too far from the cone heater. For this reason, the position of the cone heater was modified to 21.4 mm for the samples, including the WRB to meet the criteria of 25 mm between the specimen and the cone heater.

For the calculation procedure, the considered ambient temperature in the fire laboratory was defined at 21°C. The emissivity values for the WRB as well as for the composite of WRB and stone wool were unknown. The exposed material to the irradiance of the cone heater was in

both cases, the WRB; therefore, the considered emissivity was taken for rubber at 0.95 [100,101]. The same emissivity value was also applied for the samples that were composed of WRB and stone wool.

Based on the experiments that were conducted by Janssens & Gomez, the convection coefficient is relatively independent of the heat flux values that are in the range of 10 and 75 kW/m^2 with convection coefficients only varying between 13.5 to 16.0 W/m^{2}K. For the calculation procedure, the values of the convection coefficients that were considered are presented in Table 4 [95].

***Table 4**: The considered convection coefficients at different heat flux values [95]*

The heat flux [kW/m^2]	The convection coefficient [W/m^{2}K]
20	13.4
25	13.3
30	13.7
35	14.2
50	15.0

5.3 Intermediate-scale test ISO 13785-1

The intermediate-scale test ISO 13785-1 is used for estimating the fire performance of different installed materials and the construction of façades. The entire façade system is exposed to the heat source that is representing an external fire with flame impinging onto the façade [102]. The experimental set-up of the intermediate-scale test is defined in the standard ISO 13785-1:2002 and can be observed in Figure 14. The test specimen is a corner configuration composed of a back and side wall that has an angle 90° between them and is attached to the sample holder [102,103]. However, the experimental set-up does not only consist of the test specimen but also includes the support frame that is composed of three walls. As can be seen in Figure 14, the support frame includes a back wall and two draught screens. Both draught screens are positioned on each side of the back wall perpendicular to each other, while the test specimen is in the middle of the back wall. In Figure 14, all the measurements are written in millimetres; therefore, the test specimen has the back wall with a length of 1200 mm, the side wall with a width of 600 mm, while the height of the test specimen is 2400 mm. All the walls that are part of the support frame have a height of 2800 mm. The length of the back wall is 2400 mm, while the draught screens have a width of 2400 mm. The draught screens should be composed of non-combustible boards and should reach the floor to prevent air gaps [102]. As it can be observed in Figure 14**,** the test specimen is positioned 250 mm above the upper edge of the 100 kW sand-diffusion propane burner, which has a length of 1200 mm, a width of 100 mm, and the height of 150 mm [47,102]. The heat flux meter is positioned in a square non-combustible insulation board with the

dimensions of 200 x 200 mm and thickness of at least 25 mm on the upper edge of the back wall. The insulation board also contains the aperture that is positioned 30 mm above the bottom edge and has a diameter of 25 mm. The burner is located on the floor and is required to be aligned with the edges of the test specimen [102].

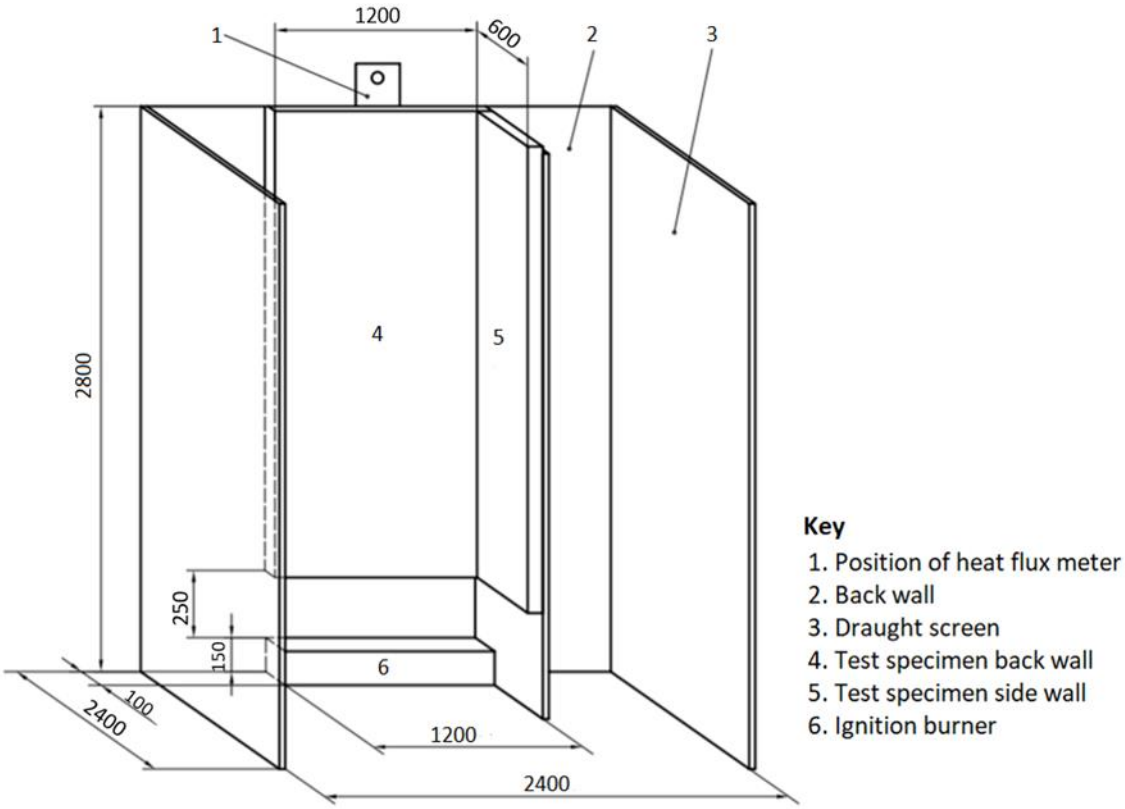

***Figure 14**: Experimental set-up as defined in ISO 13785-1 modified from [102]*

For the execution of the intermediate-scale tests, the following deviations from the standard will be made [47,55]**:**

- The burner will be turned on throughout the entire duration of the tests.
- The test duration will be 30 min, and it will not be terminated even when the flames will be flaming on top of the test specimen
- The experiments will be carried out under the calorimetric hood with the dimensions 3 x 3 m, which can measure the heat release rates up to 3 MW. During the experiments, the heat release rates will be continuously measured according to ISO 24473:2008 [104].
- The sides of the test specimen will be open.
- The insulation was at the bottom of the test specimen protected from the immediate flames from the burner by an L shape rail that can be observed in the cut-view in Figure 15.
- The thermocouples will also not be placed on the surface of the external cladding panels; however, their position can be observed in Figure 15.

5.3.1 Description of the intermediate-scale test set-up

The intermediate-scale tests were conducted at the cavity width of 100 mm with three different material compositions, as presented in Table 5. The tests involved calcium silicate boards as the external cladding panels that could be represented in the construction of façade systems with fibre cement boards due to their shared incombustibility. On the façade system were applied the same type of WRB and insulation materials that were tested in the cone calorimeter. The approximate density values of calcium silicate board and WRB were calculated based on the provided information from their producers, that the weight of calcium silicate boards is 4 kg/m^2, while the WRB has the weight of 270 g/m^2 [88,105].

***Table 5**: Material composition of the tests*

Test	Testing materials	Thickness [mm]	Density [kg/m^3]
1	External cladding panels: **Calcium silicate board**	9	428
	Insulation material: **Phenolic foam**	50	35
	WRB: **Not applied**	Not applicable	/
2	External cladding panels: **Calcium silicate board**	9	428
	Insulation material: **Stone wool**	100	45
	WRB: **Not applied**	Not applicable	/
3	External cladding panels: **Calcium silicate board**	9	428
	Insulation material: **Stone wool**	100	45
	WRB: **Self-adhering membrane**	0.5	540

The test set-up consisted of 3 x 2 panels that are positioned on the back wall with 3 additional panels on the side wall as can be observed in Figure 15. The width of the panels varied between the tests to achieve the 20 mm gap between the panels; however, the height of all the panels was defined at 779 mm. The external cladding panels for test 1 consisted of three panels that had the dimensions 600 mm x 779 mm on the back wall, while the other three panels measured 450 mm x 779 mm. The panels on the side wall had the dimensions of 430 mm x 779 mm. In test 2 on the back wall, the external cladding panels consisted of three panels measuring 545 mm x 779 mm, and the other three had the dimensions of 400 mm x 797 mm. On the other hand, the external cladding panels on the side wall measured 440 mm x 779 mm. In test 3, which included stone wool as well as the WRB included three external cladding panels, which measured 490 mm x 779 mm on the back wall, while another three panels measured 470 mm x 779 mm. On the other hand, the external cladding panels on the side wall measured 370 mm x 779 mm.

In Figure 15, a schematic representation of the thermocouple locations and the position of the heat flux gauge can be observed. All the dimensions are written in millimetres. In total, there were 50 thermocouples of type K implemented in the façade system. The thermocouples measured the temperature in the middle of the cavity width as well as the temperature in the middle of the insulation material. In Figure 15, the back and side wall represent the thermocouple locations; however, each of them had installed two thermocouples, one in the insulation material and the second one in the cavity. Even though the corner is not demonstrated, there were also in total, ten thermocouples installed on the same heights, as presented in Figure 15. The temperatures of the thermocouples were considered for the calculation of the flame height surface area during the test with stone wool. The flame height surface area only correlates to the positions of the thermocouples during the test. Flaming was considered, in case the temperature of the thermocouple was above 100°C.

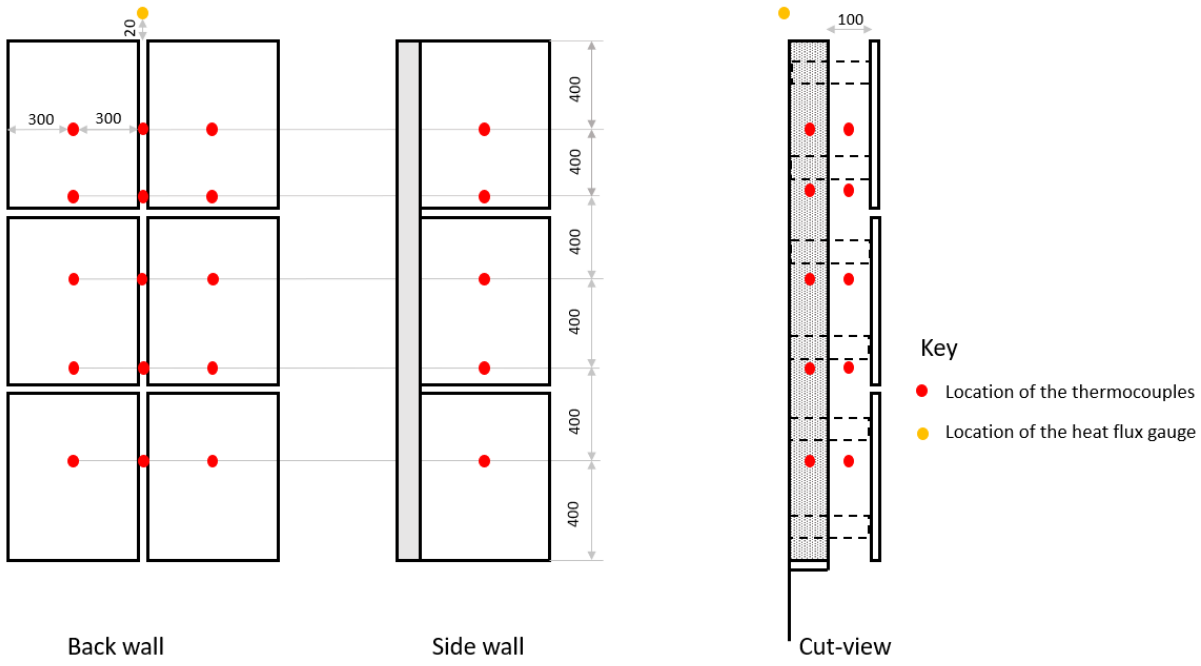

***Figure 15**: Schematic representation of instrumentation modified from [47]*

The construction process of test 2, which included stone wool as the insulation material can be seen in Figure 16. In the first step, the 12 mm thick calcium silicate boards were placed on the steel frame, followed by aluminium brackets that determined the cavity width and supported the external cladding panels. In step two, the insulation material was fitted onto the sample by making openings for the brackets. In step three, the insulation was fixed to the 12 mm calcium silicate board. In the same step, the L and T shape rails were placed onto the brackets that created the cavity width of 100 mm. In step four, the external cladding panels were attached to the L and T shape rails in the form of 9 mm thick calcium silicate boards. In a similar manner were constructed also test 1 and test 3.

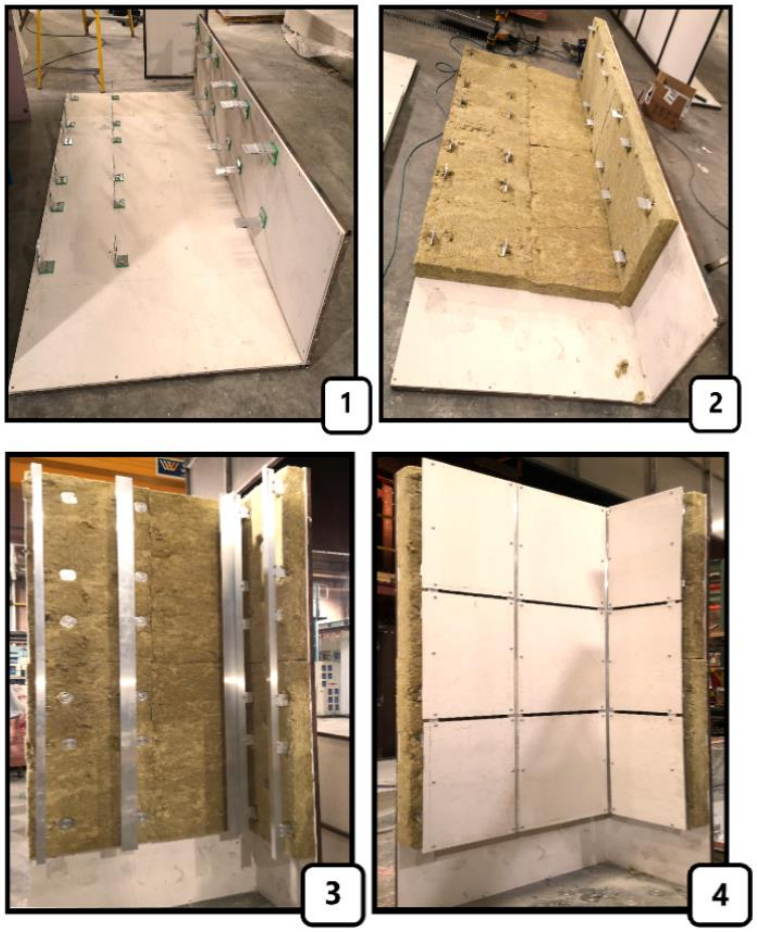

***Figure 16**: Construction process of test 2*

A comparison between all three constructed tests can be observed in Figure 17. As already mentioned, all three experiments had the cavity width of 100 mm and only varied between each other based on the material that was exposed to the air cavity.

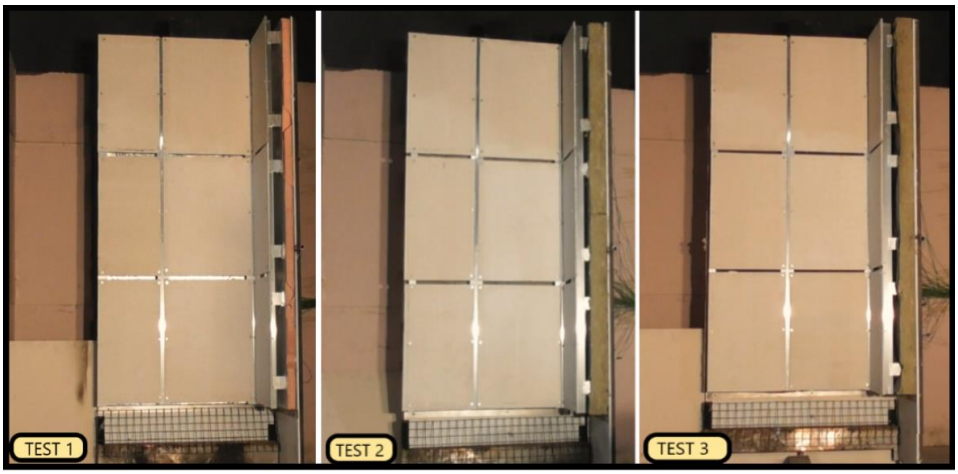

***Figure 17**: All three constructed façade systems*

6. Results and discussion

6.1 Cone calorimeter tests

Before testing, all the samples were wrapped in the single layer of aluminium foil as described in the standard [91]. The specimens had the size of 100 mm x 100 mm; however, due to the lack of WRB material, some of the samples had the size of 100 mm x 87 mm that would need to be accounted for in the calculation of the heat release rate. The surface area that the cone calorimeter considers for the calculation of the heat release rate is based on the 94 mm x 94 mm samples, that have the exposed surface area of 88.36 mm^2. However, due to some smaller samples, the surface area that would be exposed to the cone heater would need to be recalculated for the estimation of the heat release rate.

The maximum heat release rates of the tested WRB, K-Roc, and K15 at different heat flux levels are presented in Table 6. Stone wool that was tested at 50 kW/m^2 had the maximum heat release rate of 10 kW/m^2 and, therefore, the lowest heat release rate among all the seven tests. The material during the test did not ignite, and due to the low heat release rate, the test with the stone wool was not repeated at lower heat fluxes. The maximum heat release rates for WRB varied only for approximately 29 kW/m^2 between each other based on the applied heat flux. The results obtained at the heat flux of 35 kW/m^2 included WRB and K15. However, even though the Euroclass of WRB is defined as B, while K15 is classified as class C, the WRB had the maximum heat release rate higher for 63 kW/m^2. This could be explained, due to the phenolic foam being tested without the external aluminium facing that would otherwise base on the literature [70] affect the result.

***Table 6**: Maximum heat release rates of K-Roc, WRB and K15*

Test	Tested material	Heat flux [kW/m^2]	Maximum HRR [kW/m^2]
1	K-Roc	50	10
2	WRB	50	128
3	WRB	35	127
4	WRB	30	99
5	WRB	25	103
6	WRB	20	104
7	K15	35	64

In the literature [37] the densities of stone wool can range up to 200 kg/m^3; therefore the test 1 which consisted of testing K-Roc with a density of 45 kg/m^3 classifies as the material with a lower density. The maximum heat release rate that was attained during the test demonstrated that the value only varied for around 4 kW/m^2 from the test which tested the stone wool with a density of 37 kg/m^3 at the same heat flux of 50 kW/m^2 [46]. Therefore, it is

assumed, that the results that were conducted with the stone wool at the density of 40 kg/m^3 could be applicable for K-Roc and the material would most likely not ignite even up to the heat fluxes of 88 kW/m^2 [70].

The maximum HRR value of test 7 can be compared to the value found in the literature for phenolic foam that was also tested at the heat flux of 35 kW/m^2 with similar thermal properties [70]. The density of the phenolic foam determines the ratio of the closed cells within the material that also influence other characteristics of the foam [78]. Therefore, the comparison between the two phenolic foam was only made due to the low-density difference of approximately 3 kg/m^3. The maximum heat release rate for K15 at the heat flux value of 35 kW/m^2 was estimated at 64 kW/m^2, while on the other hand, the second phenolic foam had a maximum heat release rate of around 60 kW/m^2. Therefore, the difference between the maximum heat release values was estimated to be at approximately 6.1 %. As part of further research, the K15 should be tested at different heat flux values for a better comparison with the literature values.

For the estimation of the surface temperature increase, the thermal inertia was estimated for the phenolic foam in the literature between 1.35 and 1.2 W^{2}s/m^{4}K^2, that differed from the thermal inertia for K15 for approximately 3.7 to 12.4 %. For this reason, it could be assumed that the surface temperatures of both phenolic foams would be closely correlated.

The heat release rates as a function time are presented for all the seven tests in Figure 18. The results are shown only for the period of 180 s, due to the quick ignition of the materials, which consequently lead to the attainment of their maximum heat release rates. As it can be observed, the range of applied heat fluxes to the WRB did not have a considerable effect on the maximum heat release rates of the material. However, with the reduction of heat fluxes, the time that's required for the material to reach the maximum heat release rate is prolonged. For this reason, the time difference of 42 s can be observed between the test 1 that was conducted at the heat flux of 50 kW/m^2 and test 6, which was exposed to the heat flux of 20 kW/m^2.

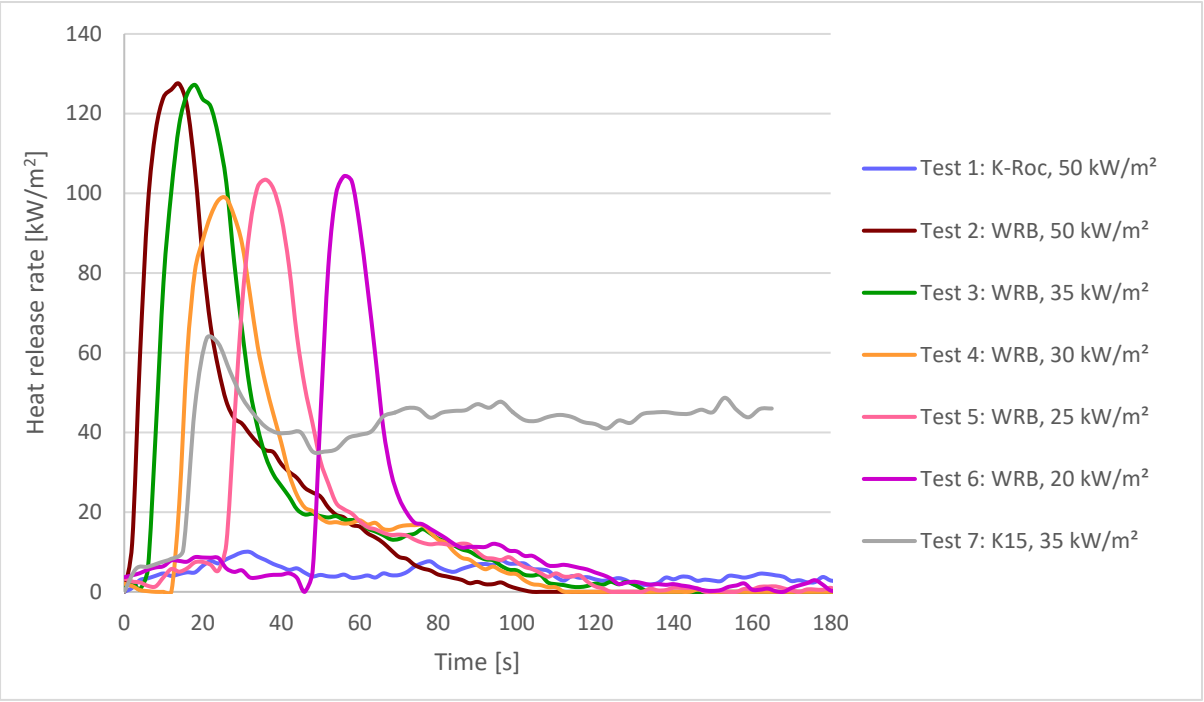

***Figure 18**: Heat release rate as a function of time for stone wool, WRB and phenolic foam*

In the cone calorimeter, also five tests were executed that were composed of WRB that was placed on top of the stone wool as it can be seen in Figure 12. In Table 7, the tested composites are presented; their heat flux values as well as the maximum heat release rates. When comparing test 8 and test 10, the maximum heat release rates differ for around 39 kW/m^2. However, the heat flux difference of 5 kW/m^2 that was present between test 9 and test 10 did not result in the lower maximum heat release rate. The composite was tested at the heat flux of 25 kW/m^2 twice because the material did not ignite during test 11. For this reason, the test was repeated at the same heat flux, to confirm whether the critical heat flux was reached. However, in test 12, the composite ignited and reached the maximum heat release rate of 73 kW/m^2, which is compared to test 8, approximately 71 kW/m^2 lower.

***Table 7**: Maximum heat release rates of WRB and stone wool composites*

Test	Tested composite	Heat flux [kW]	Maximum HRR [kW/m^2]
8	WRB and stone wool	50	144
9		35	105
10		30	105
11		25	21
12		25	73

The heat release rates as a function of time for all the five composites are presented in Figure 19, from which it can be observed that the curves of heat release rates for test 9 and test 10 are almost identical. As can be seen, the time to reach the maximum heat release rate between different tests did not differ as significantly as in the results presented in Figure 18.

The highest difference between the times that were required for the materials that ignited to reach their maximum heat release rate was observed in test 8 and test 12, which was estimated to be 10 s.

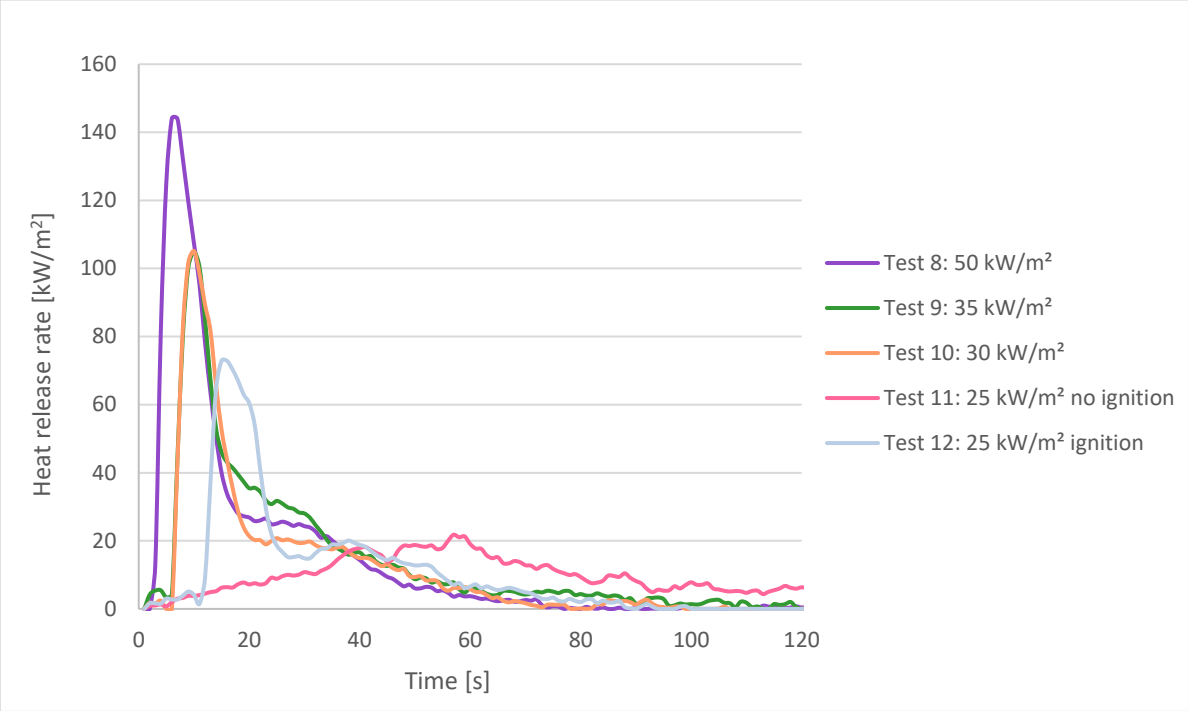

***Figure 19**: Heat release rate as a function time for WRB and stone wool composite*

Based on the least-square method, the tests involving the WRB material as well as the tests that were composed of the WRB and stone wool composite classified as thermally thick materials. At the value of $n = 0.55$ the R^2 value for the WRB tests corresponded to 0.9801, while at $n = 1$ the R^2 was estimated to be 0.8367. Similarly, the tests that included the WRB and stone wool had the R^2 value at $n = 0.55$ defined as 0.9375 and at the n value of 1, the R^2 was defined at 0.8234. Even though the thickness of the WRB is only 0.5 mm, the material was classified as thermally thick due to the correlation with the literature; therefore, additional experiments would be required to classify the material as thermally thin [74,96].

The correlation between the times to ignition as a function of heat flux for WRB as well as for the composite of WRB and stone wool is presented in Figure 20. The critical heat flux values for both samples were estimated based on the intercept of the lines with the abscissa. For WRB, the critical heat flux value was determined at 8.57 kW/m^2 and for the composite material of WRB and stone wool at 2.65 kW/m^2.

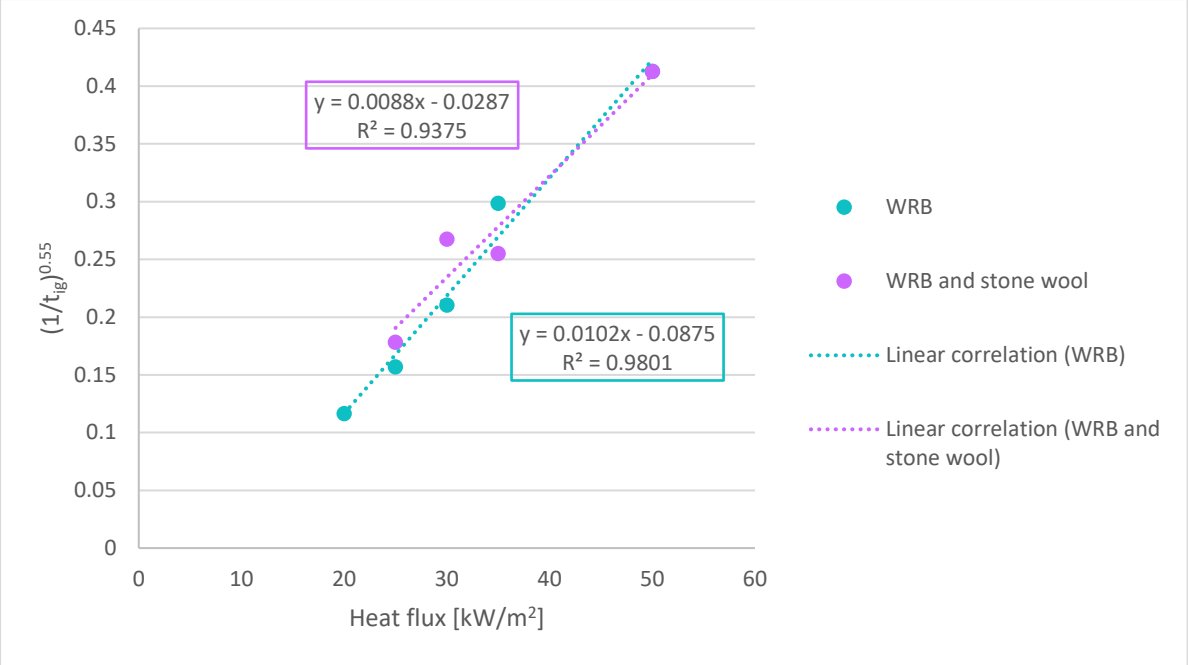

***Figure 20**: Time to ignition as a function of heat flux for WRB and the WRB and stone wool composite*

The average calculated surface temperature at the time of ignition for the WRB was 273°C with the highest variation of 8.2°C between the surface temperatures due to applied different convection coefficients. On the other hand, the average calculated surface temperature for the composite of WRB and stone wool was approximately 128°C, with the highest difference between the temperatures of 6.6°C.

The calculated thermal inertias for WRB and the WRB and stone wool composites at different applied heat fluxes are presented in Table 8. As it can be observed, the thermal inertias for the WRB samples are a few times smaller compared to the thermal inertias of the composite. The highest difference between the thermal inertias for the two samples was calculated for the applied heat flux of 35kW/m^2, which was estimated to be at around 8.9 times. On the other hand, the smallest difference was observed at the heat flux at 30 kW/m^2 at 4.6 times.

***Table 8**: Calculated thermal inertia for WRB and the WRB and stone wool composite*

The applied heat flux [kW/m^2]	**Calculated thermal inertia [W^{2}s/m^{4}K^2]**	
	WRB	**WRB and stone wool**
50	0.16	0.99
35	0.13	1.12
30	0.16	0.73
25	0.17	1.02
20	0.15	/

As already mentioned, the thermal inertia is correlated to the surface temperature and determines its increase; therefore, the surface temperature of WRB should be significantly higher compared to the surface temperatures of the composite. This can be observed from

the comparison of the calculated averaged surface temperature for the WRB that is approximately 149.5°C higher than the surface temperature of the composite sample.

The thermal inertia was also calculated for the stone wool at ambient temperature based on the information provided in Table 3 and was estimated to be 1.53 W^2s/m^4K^2. Therefore, the WRB contributes to the quicker increase of the surface temperature for approximately 33.4% to 47.7%.

6.2 Intermediate-scale tests

The analysis of the results will consist of the tests that were carried out during this master's thesis; however, it will also include the results of the other intermediate-scale tests ISO 13785-1:2002 tests that were executed in the same fire laboratory by different researchers. The tests from number 4 to 7 that can be observed in Table 9 were already presented in [47,55]. On the other hand, test 8, test 9 and test 10 are considered and analysed with the consent from Kingspan.

The intermediate-scale tests will be examined based on the performance of the overall façade system as well as by estimating the influence of individual components that were identical in different tests. The individual components will be examined to contribute to already existing knowledge regarding the influence of individual components on the heat release rate of the entire façade system. Even though based on the literature [21,47] the fire behaviour of the façade system depends more on the overall performance of the entire system rather than on individual components.

The tests that will be included in the analysis consist of different material compositions at various cavity widths, as presented in Table 9. The tests varied between each other by implementing different external cladding panels, changing the insulation materials as well as by modifying the cavity width. All the tests, except number 8, were executed with the cavity barriers that were installed at the height of 1.6 m and prevented the vertical flame spread within the cavity.

In test 4 and test 5, the external cladding panel ACM-A2 was aluminium composite material, which had the included core material that consisted of 90% non-combustible material. The external cladding panel of test 6 and test 7 was ACM-FR which was composed of aluminium composite material and had 70% of the core material of non-combustible material. For test 8, the external cladding is defined as a polymer that had a core material of crushed natural stone and is defined by Euroclass as class B-s1,d0. On the other hand, tests 9 and 10 had the external cladding panel of natural stone that is incombustible. Five of the tests included phenolic foam K15 as the insulation material, while stone wool was applied in test 4 and test

6. As can be observed from Table 9, the cavity width differed between the tests from 38 mm cavity that was present for the test 8 to 100 mm cavity for test 10.

***Table 9**: Material composition of various intermediate-scale tests*

Test	External cladding panel	Insulation material	Cavity width [mm]
4	ACM-A2	Stone wool	50
5	ACM-A2	K15	50
6	ACM-FR	Stone wool	50
7	ACM-FR	K15	50
8	Polymer	K15	38
9	Natural stone (NS)	K15	40
10	Natural stone (NS)	K15	100

In Figure 21, the heat release rate (HRR) as a function of time is presented for the material compositions that are defined in Table 9. The burner influence of 100 kW was deducted from the heat release rates, and the assumption of the constant flow rate was considered. The comparison between the maximum heat release rates of all the seven tests is presented in Figure 22.

As it can be observed from Figure 21, the lowest heat release rate is present for test 9 with the natural stone at 40 mm cavity, while one of the highest maximum heat release rates is present for the test 8 with the polymer material as the external cladding panel at the cavity width of 38 mm. Even though the tests had the same type of insulation and their cavity width only varied between the two tests for 2 mm, the maximum heat release rate of test 8 was almost 235 kW higher than of test 8. The material compositions of test 5 and test 7 had similarly K15 as an insulation material, while the external cladding panels of test 5 included ACM-A2 and in test 7 ACM-FR. The change of the external cladding material from ACM-A2 in test 5 to ACM-FR in test 7 increased the maximum heat release rate for approximately 134 kW. The results demonstrated that the substantial influence of external cladding panels on the heat release rate could perhaps be extended from ACM cladding panels to other types of external cladding panels. However, to confirm this statement, additional experiments would need to be conducted.

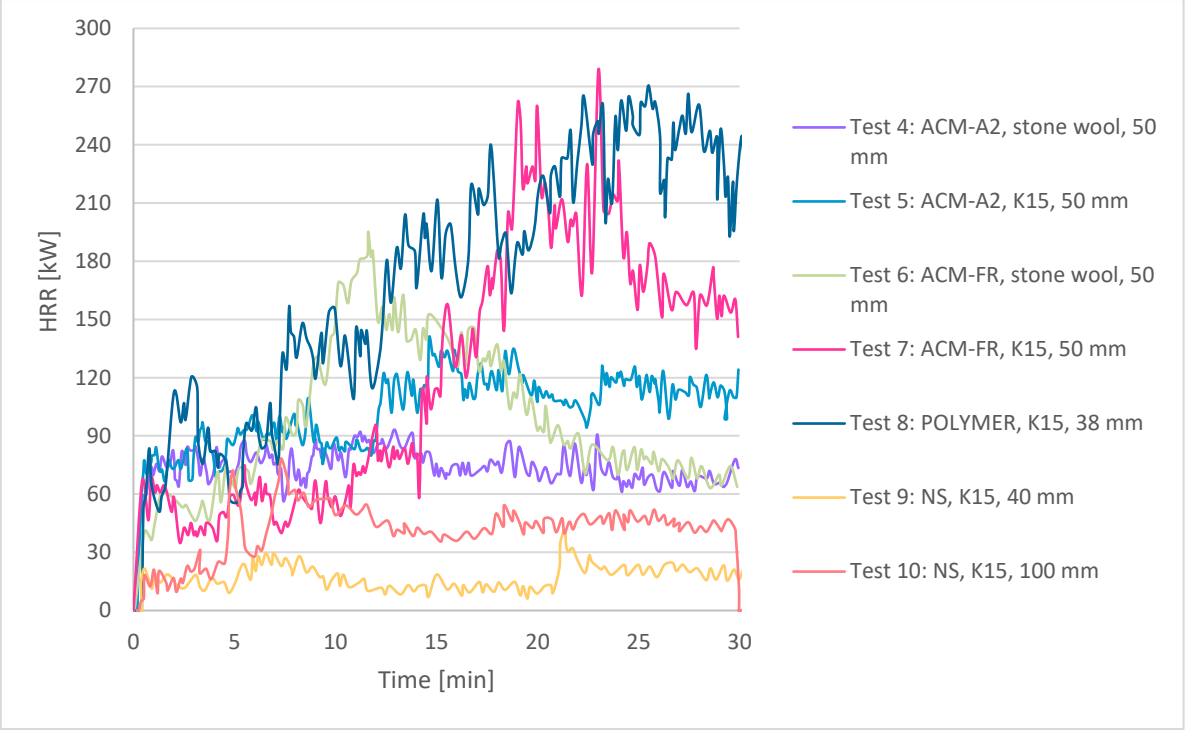

***Figure 21**: Heat release rate as a function of time for various façade systems*

Test 4 and test 5 were executed at the cavity width of 50 mm, with the only distinction between the tests in the installation of the insulation material. As it can be observed from Figure 22, the phenolic foam has a higher heat release rate with the maximum difference from stone wool for approximately 50 kW. In a similar manner test 6 and test 7 that were also conducted at the cavity width of 50 mm with the only variation in the insulation material demonstrated, that the phenolic foam insulation contributed approximately 83 kW more to the maximum heat release rate. The effect of the insulation was only compared for the cavity width of 50 mm and two different types of external cladding panels; therefore, additional experiments would be required to make any further conclusions.

In test 9 and test 10 can be observed the influence of the cavity width on the heat release rate, as the tests are composed of the same external cladding panels and insulation materials. The results demonstrate that the increase of the cavity width from 40 mm to 100 mm also exhibits a higher energy release. For this reason, test 10 has the maximum heat release rate that is approximately 36 kW higher than at the cavity width of 40 mm.

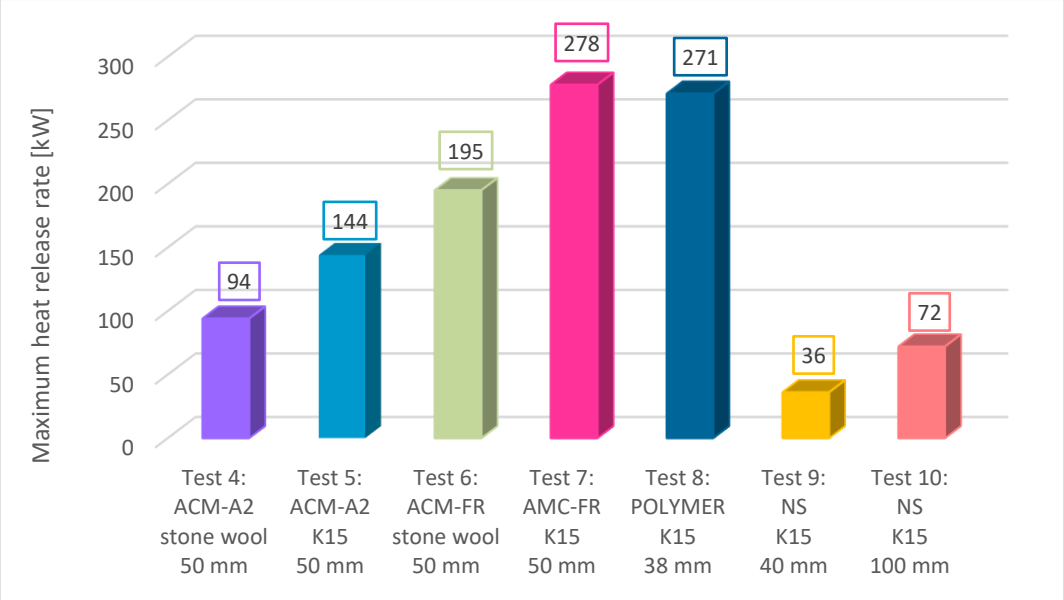

***Figure 22**: Maximum heat release rate of all the five tests with the applied moving average technique*

For a better understanding of the cavity width influence on the heat release rate as well as on the heat flux, three additional intermediate-scale tests were executed at the cavity width of 100 mm, as presented in Table 10. In a similar manner as for previous tests, the burner influence of 100 kW was deducted from the heat release rates and the assumption of the constant flow rate was considered. The experiments had installed incombustible external cladding panels as test 9 and test 10; however, they were tested without the cavity barriers and with open sides.

***Table 10**: Material composition of three executed intermediate-scale tests*

Test	External cladding panel	Insulation material	Cavity width [mm]
1	Calcium silicate board	K15	100
2	Calcium silicate board	K-Roc	100
3	Calcium silicate board	K-Roc with WRB	100

In Figure 23, the heat release rate as a function of time for all the three executed tests can be observed. Based on the cone calorimeter results and the Euroclass system, the test with K-Roc has as expected the lowest heat release rate of all the three tests. The K15, as well as the composite of WRB and stone wool, were both tested in the cone calorimeter at the heat flux of 35 kW/m^2. Based on the cone calorimeter results, the maximum heat release rate of the WRB and stone wool composite is approximately 1.7 times higher compared to K15. Even though the K15 was tested without the protective aluminium foil facing it would still be expected that the overall heat release rate of test 3 would be significantly higher than of test 1. However, this conclusion based on Figure 23 cannot be made.

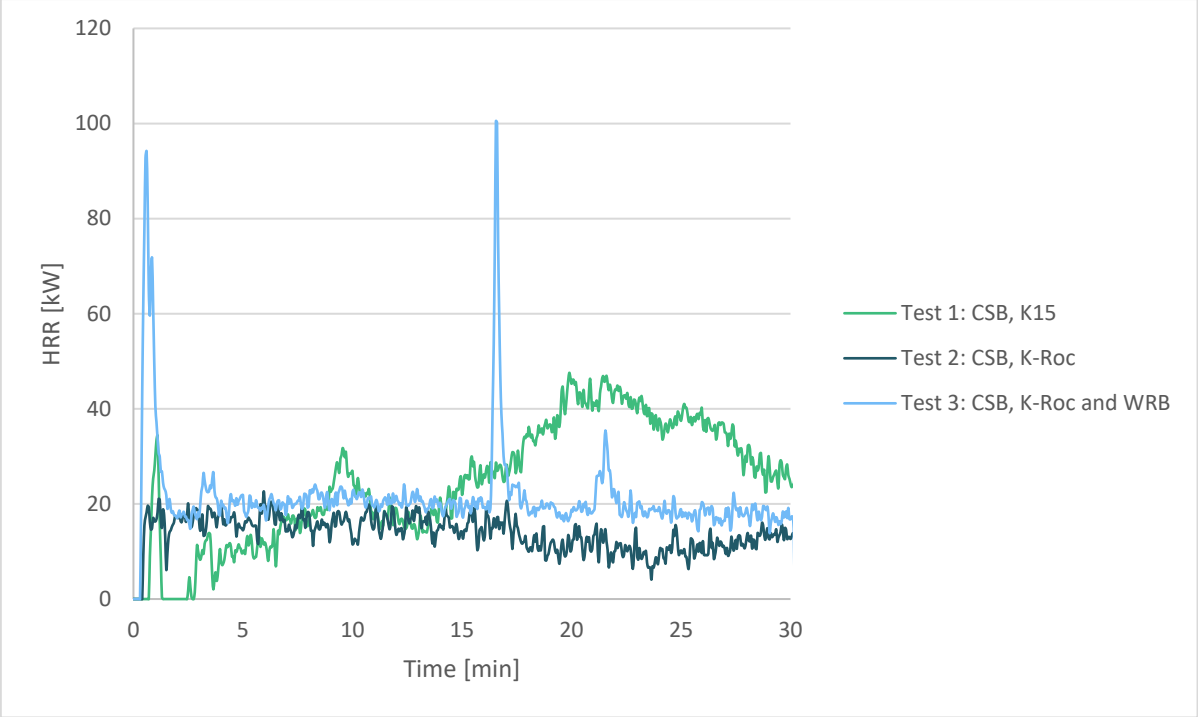

***Figure 23**: Heat release rate as a function of time for executed façade systems*

During the execution of the intermediate-scale tests, the flame heights of all three tests were recorded by a video camera. The presented heat release rates of all three tests correspond to the observed flaming during the tests. In Figure 24, Figure 25 and Figure 26 two times during the tests are presented, where the increase of heat release rate was recognized. In Figure 24, the flaming above the experimental set up of test 1 can be observed at 26 s and 19.35 min, which correspond to higher heat flux values. At the time of 26 s, the flames disappeared above the set-up in a few seconds. On the other hand, as the test continued, the flames shifted towards the corner where there is less air entrainment, and at approximately 19.35 min the flames continued to be above the rig for around 8 minutes.

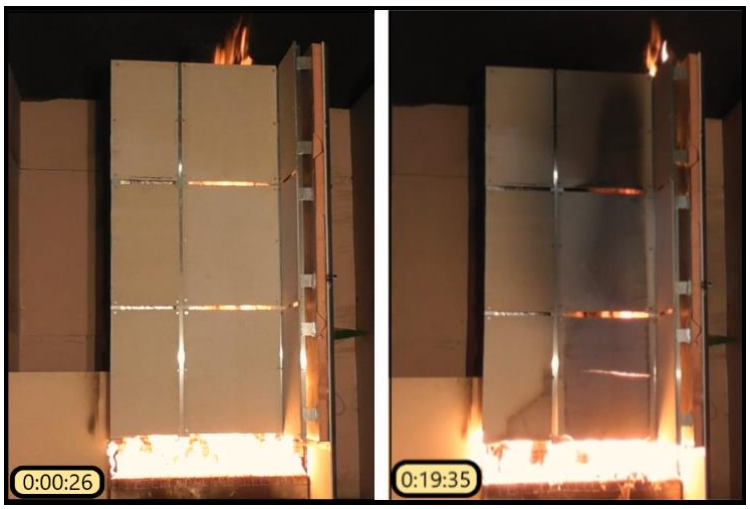

***Figure 24**: Observed flame heights of test 1: CSB, K15*

The flame heights of test 2 which included the K-Roc, never exceeded the height of 1.6 m during the test and as it can be observed from Figure 25, the flame heights at two different time period are quite consistent.

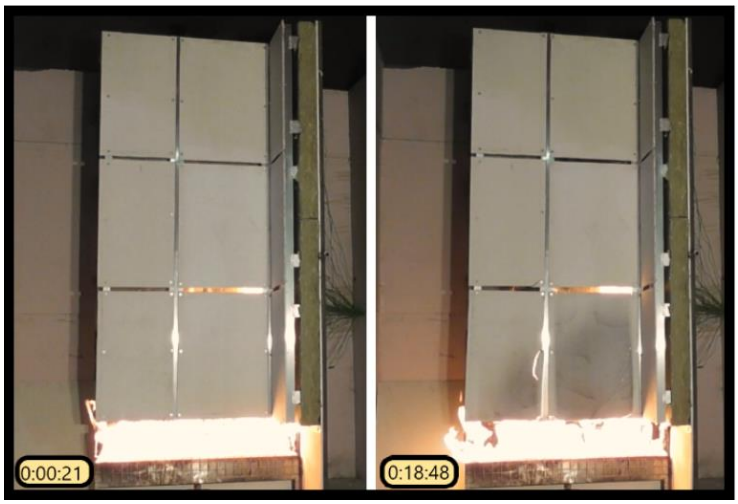

***Figure 25**: Observed flame heights of test 2: CSB, K-Roc*

The heat release rate of test 3 consists of two high peaks of 90-100 kW, which correlate to the flaming that was present at the time on top of the experimental set-up as presented in Figure 26. The WRB material, especially at the beginning of the test started melting, which increased the flame height at around 21s. However, as the test proceeded, the flames shifted towards the corner as in test with K15. The WRB material in the corner then started to melt and drip, which resulted in a high heat release rate.

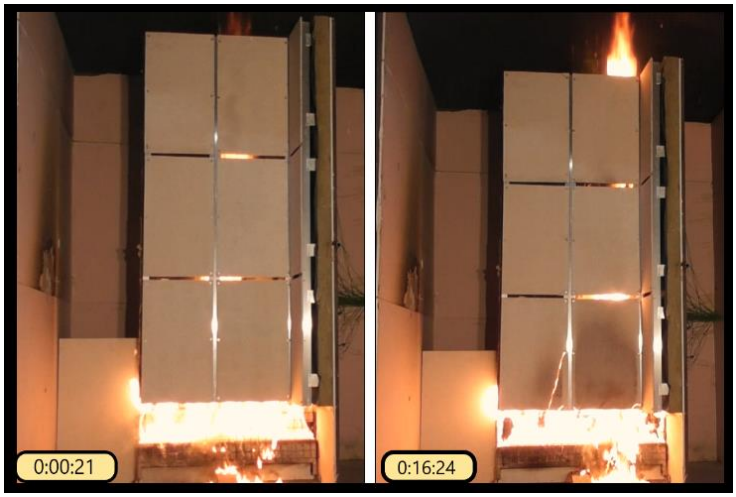

***Figure 26**: Observed flame heights of test 3: CSB, K-Roc and WRB*

In Figure 27, the maximum heat release rates for the three executed tests are presented. The correlation between the maximum heat release rates of K15 and composite of stone wool and WRB that was observed in the cone calorimeter is also present in the intermediate-scale tests. The maximum heat release rate of K-Roc and WRB composite is approximately 2.1 times higher compared to the K15.

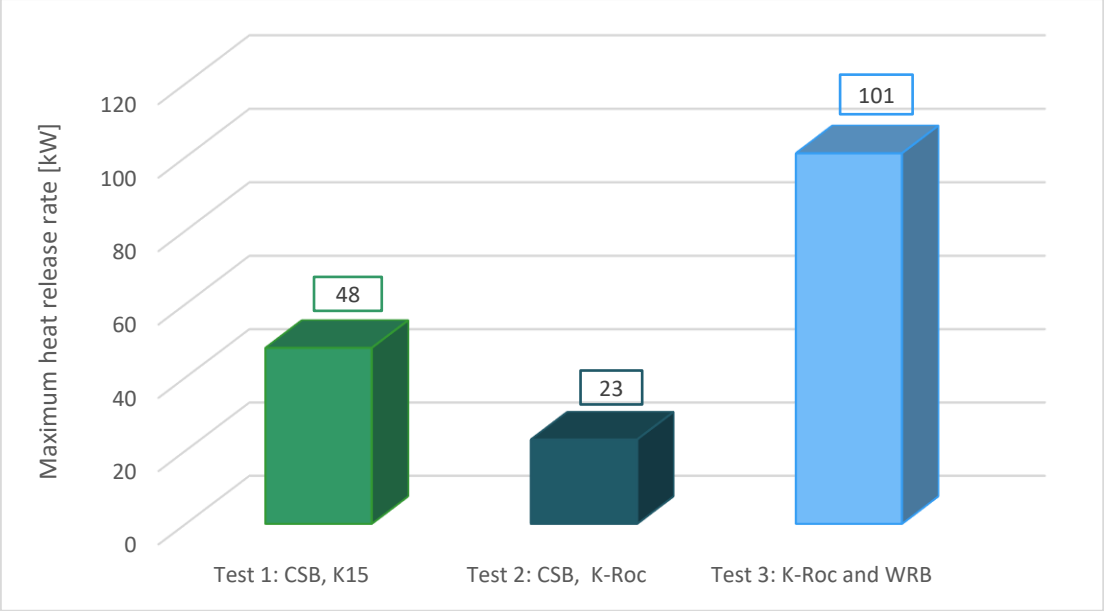

***Figure 27**: Maximum heat release rate for all the three executed tests*

Burning within a cavity is defined by the chimney effect and the limited air supply for the combustion process [21]. Test 1 and test 10 were both executed at the cavity width of 100 mm, with K15 and incombustible external cladding panels. The only distinction between the tests was the implementation of the cavity barrier in test 10, which limited the vertical flame spread and the oxygen conditions on the sides of both specimens. In test 1, the heat release rate throughout the test did not exceed 48 kW, while in test 10, the maximum heat release rate was estimated at 72 kW. For this reason, it can be concluded that in test 1, due to the open sides, the air supply was unlimited, and the chimney effect was reduced. As part of the further research, it would be beneficial to conduct additional experiments at smaller cavity widths and different oxygen conditions, by modifying the openings on the sides of the test specimens.

The combined effect of radiation and convection was measured during the tests with the heat flux gauge, which was positioned as presented in Figure 14 and to reduce the fluctuations of the measurements the moving average technique was applied for the period of every 12 s. The heat flux values as a function of time are presented for all the four tests with a cavity width of 100 mm in Figure 28. The intermediate-scale test ISO 13785-1 exposes the façade to an approximately 50 kW/m^2 by using a 100 kW propane burner. As already mentioned, the measured heat flux is dependent on the distance between the heat flux gauge and the heat source, which is estimated to be approximately 2.4 m during the experiments. However, in case the flames during the experiments appear above the experimental set-up, the heat flux values will be influenced. The highest heat flux values are present for test 1, even though the measured heat release rate was higher for test 10. The implemented cavity barriers at the height of 1.6 m for test 10 prevented the vertical flame spread within the cavity. For this

reason, the heat flux gauge, which is positioned at the upper part of the back wall, measured lower heat flux values.

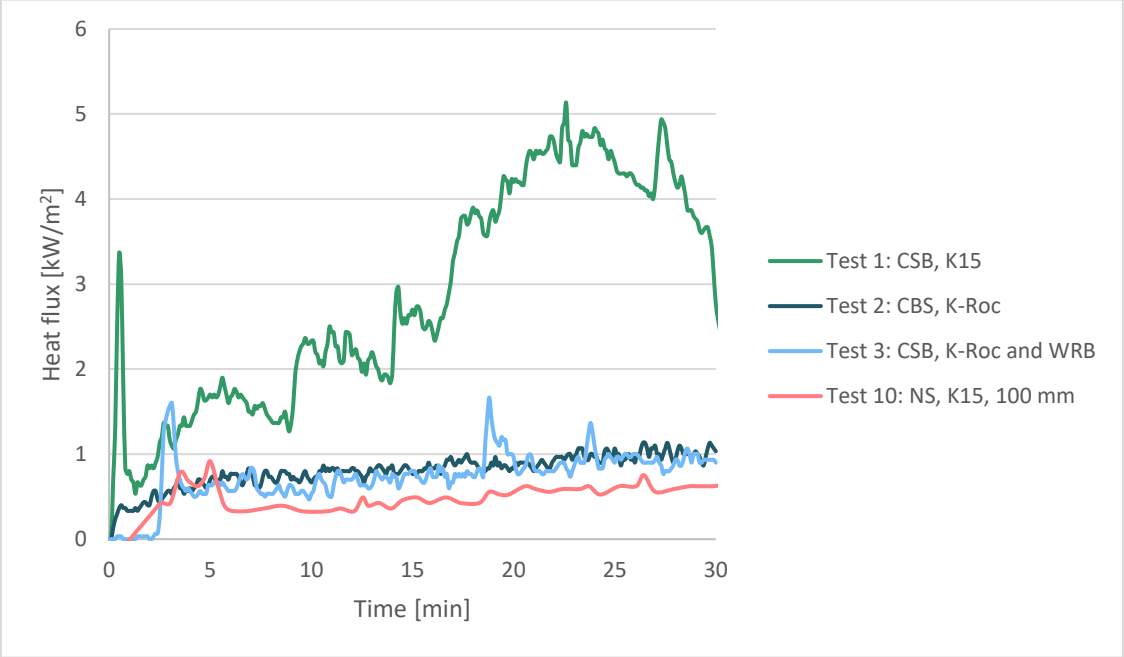

***Figure 28**: Heat flux as a function of time with applied moving average*

In Figure 29, the HRR values for stone wool that were based on two different scales of oxygen consumption are presented. Test 2 shows the HRR values that were estimated during the intermediate-scale test, while test 1 corresponds to the combination of the cone calorimeter data at 50 kW/m^2 and intermediate-scale results. The HRR values of test 1 were determined based on the heat release rates of stone wool during the cone calorimeter test while considering the approximate flame heights during the intermediate-scale test. The flame surface area during 10 minutes, in general, ranged from 1.7 m^2 to 1.9 m^2; however, the maximum surface area was estimated at 2 m^2. The correlation between the HRR values is presented for 10 minutes, and the estimation of the approximate flame heights was estimated every 10 s. From Figure 29, a similar pattern between the HRR values for the first two minutes can be observed. However, afterwards, the HRR values in the cone calorimeter started to reduce that increased the difference between the two tests, that could be correlated to the tested sample sizes. In the cone calorimeter, the tested sample has an area of 0.01 m^2; however, in the intermediate-scale test, the area of stone wool was approximately 4.3m^2.

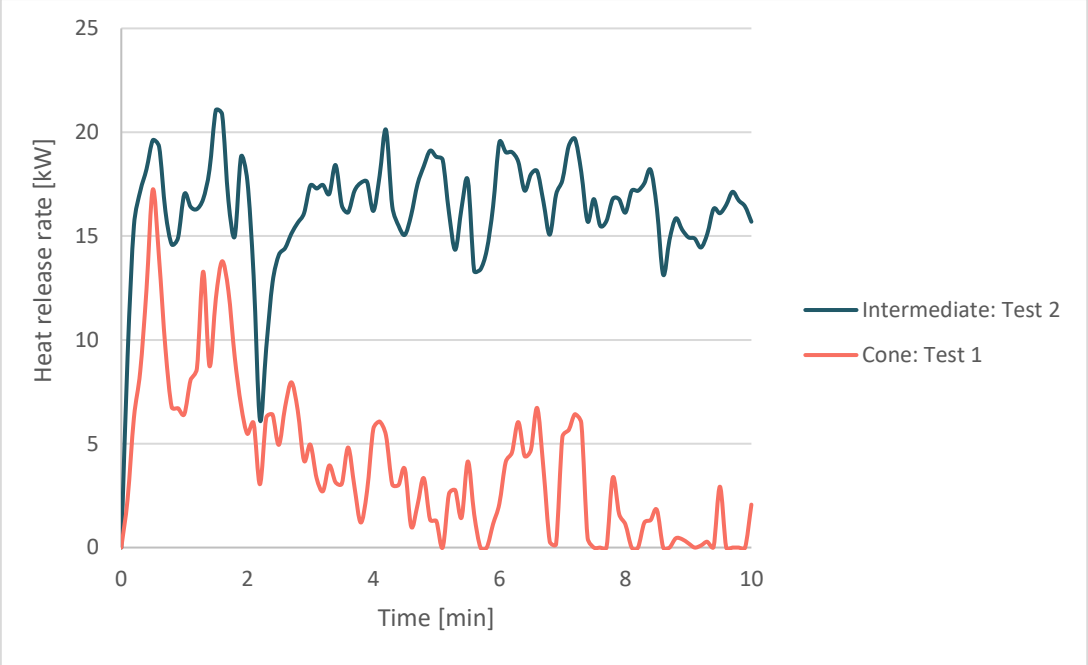

***Figure 29**: Comparison of HRR values for stone wool (cone calorimeter and intermediate-scale)*

In a similar manner, the comparison between the heat release rates of stone wool and WRB composite is presented in Figure 30. The correlation between the tests was conducted based on the results of HRR values for the intermediate-scale test 3 that were compared to the cone calorimeter data. The test that was considered from the cone calorimeter is test 8, which was exposed to the heat flux of 50 kW/m^2. The calculation procedure of the HRR values for cone calorimeter data presented in Figure 30 was identical to the procedure already described for stone wool sample in Figure 29. The HRR values are only defined for 3 minutes, due to the quick ignition time of WRB and stone wool composite in the cone calorimeter. The surface area of the flames was for most of the considered time estimated at its maximum value of 2.3 m^2. The comparison of the HRR values indicates that the values of cone calorimeter data and the intermediate-scale tests are comparable. In both cases, the material started to melt after a few seconds into the test, which resulted in high peaks of heat release rate.

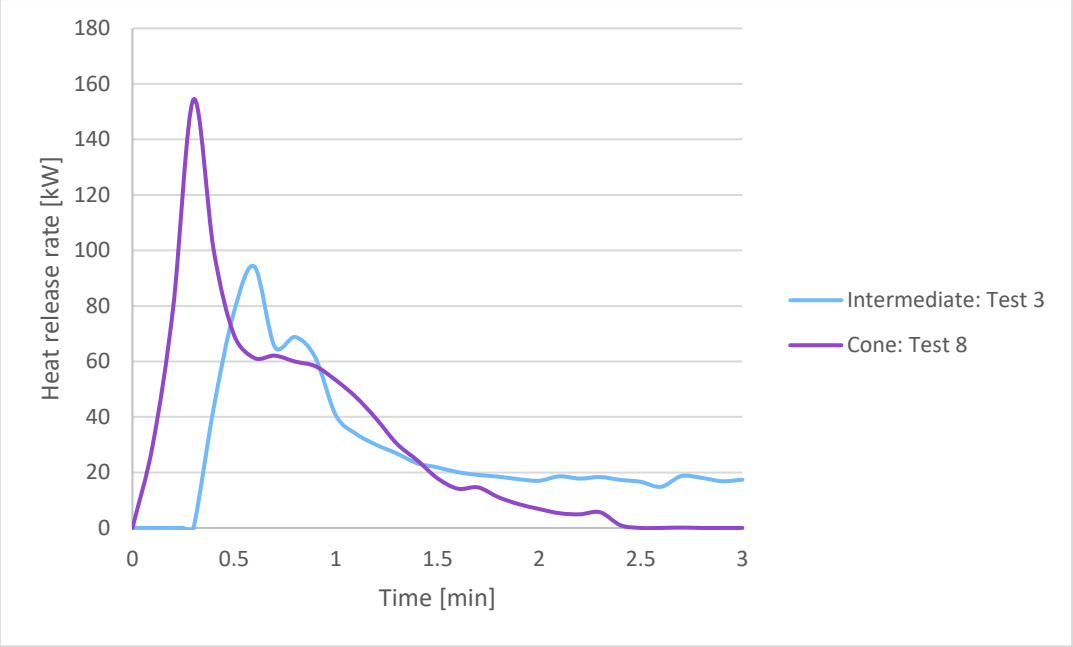

***Figure 30**: Comparison of HRR values for stone wool and WRB composite (cone calorimeter and intermediate-scale)*

In Figure 31, the heat release rate as a function of time for phenolic foam can be observed. The duration of the cone calorimeter test with phenolic foam only lasted for 2.7 minutes; therefore, the results are compared only for the duration of the test. The HRR values of the intermediate-scale experiment are presented for the period of the test. However, due to the small HRR values at the beginning of the test; the results were also compared to the HRR values that started at 19 minutes, which demonstrated a more characteristic behaviour of phenolic foam. The calculation procedure of the HRR values for cone calorimeter data presented in Figure 31 was identical to the procedure already described for stone wool sample in Figure 29. The estimated area of the flame was for the majority of times at 1.9 m^2; however, the maximum area was 2 m^2. As it can be observed from Figure 31, the values between the cone calorimeter data and the intermediate test 1 are not so comparable. However, when the cone calorimeter test data is compared to the intermediate test that was taken as a comparison at 19 minutes, the values are in a similar range. Even though the phenolic foam in the cone calorimeter was only exposed to 35 kW/m^2 and was tested without the aluminium foil covering. For any further analysis, additional experiments would be required with the phenolic foam in the cone calorimeter at higher heat flux values.

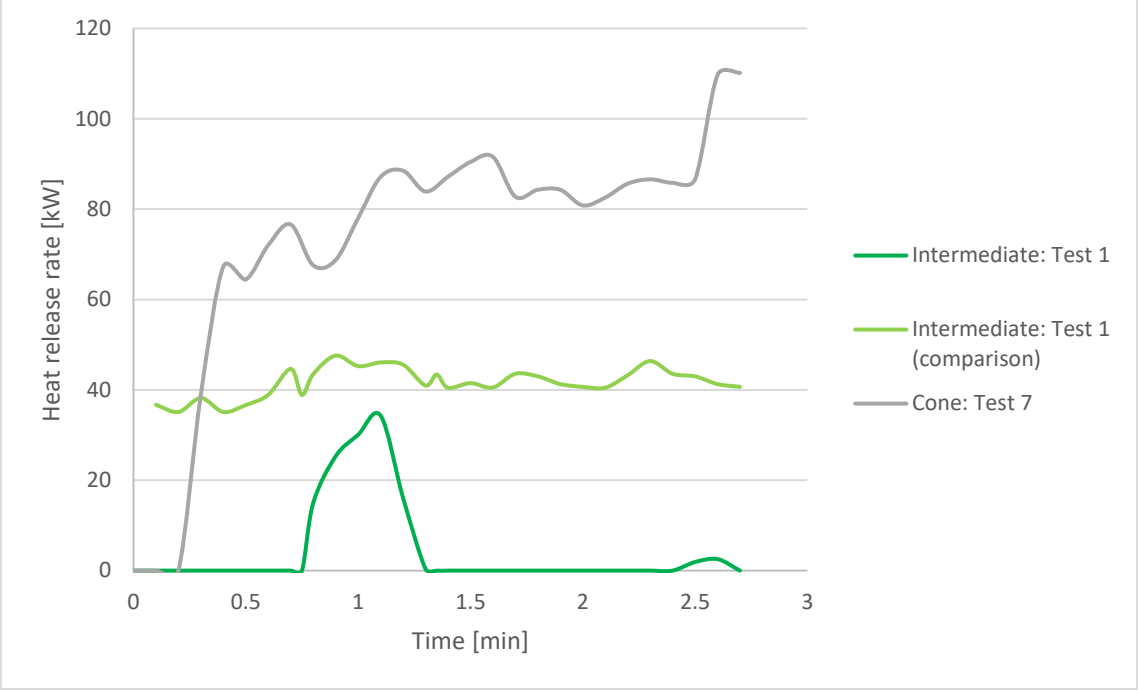

***Figure 31**: Comparison of HRR values for phenolic foam (cone calorimeter and intermediate-scale)*

The comparison between the intermediate-scale tests and the cone calorimeter tests that are presented in Figure 29, Figure 30 and Figure 31 are only roughly analysed. However, based on the results, a correlation between the intermediate-scale and cone calorimeter tests can already be observed. On the other hand, for further analysis of the results, a more advanced method would be required.

7. Conclusions

Façades represent a critical element in a building due to the plausible high energy losses that can occur through the building envelope as well as from the fire safety engineering perspective. The flames that spread into the air cavity of the façade can due to the limited airflow elongate up to five to ten times and, in addition, can be disguised due to the external cladding panels of the façade. For this reason, façade fires represent a challenge for emergency services, especially in high-rise buildings. The objective of this thesis was to provide additional information regarding the fire behaviour of three intermediate-scale façade systems. The experiments varied between each other by modifying the materials within the air cavity from K15, K-Roc to a composite of K-Roc and WRB. The results were compared to the executed cone calorimeter tests with identical materials at different levels of radiation.

The results of cone calorimeter demonstrated that the heat release rates of WRB and stone wool composite are comparable to the heat release rates of intermediate-scale test. The cone calorimeter data indicated that the WRB and stone wool composite would have relatively quick ignition times and high heat release rates at various levels of heat flux values. For this reason, the WRB and stone wool composite could be defined as a fire hazard when implemented in a façade system. Therefore, the façade systems that would have implemented WRB and stone wool composite would also require instalment of cavity barriers, that would prevent the vertical flame spread within the cavity.

The results of the intermediate-scale tests showed the importance of specific parameters within a system, such as the openness of the sides and the external cladding panels. The executed intermediate-scale experiments exhibited lower heat release rates compared to the previously executed tests due to the openness of the sides, which provided the supply of air and consequently limited the chimney effect with the height of the cavity. The influence of the external cladding panels on the maximum heat release rate was observed when modifying only the external cladding panels from natural stone to polymer material. The results demonstrated that the substantial influence of ACM external cladding panels on the heat release rate could perhaps be extended to other types of external cladding panels. However, additional experiments would be required, and the intermediate-scale results would still also need to be validated with the full-scale façade tests.

As part of the further research, it would be beneficial to conduct additional experiments at smaller cavity widths and by varying the oxygen conditions on the sides of the test specimen for a better observation of the flame spread at different cavity widths. For a better comparison of the cone calorimeter data with the intermediate-scale tests, the K15 should be tested at various heat flux values with and without the aluminium foil facing. In a similar manner, the additional cone calorimeter tests with WRB would be required to classify the material as thermally thin that would influence the critical heat flux value and the thermal inertia.

8. References

[1] L. Boström, R. Chiva, S. Colwell, I. Móder, P. Tóth, A. Hofmann-Böllinghaus, D. Lange, J. Anderson, Development of a European approach to assess the fire performance of facades, 2018. https://doi.org/10.2873/954759.

[2] I. Fu, M. Spearpoint, K. Frank, Façade Fire Incidents in Tall Buildings, CTBUH J. (2019) 34–39.

[3] P. Van Hees, M. Stromgren, B. Meacham, An holistic approach for fire safety requirements and design of facade systems, 2020.

[4] A.A. Stec, T.R. Hull, Assessment of the fire toxicity of building insulation materials, Energy Build. 43 (2011) 498–506. https://doi.org/10.1016/j.enbuild.2010.10.015.

[5] P. van Hees, M. Stromgren, B. Meacham, An holistic approach for fire safety requirements and design of facade systems, in: Proc. 15th Int. Fire Sci. Eng. Conf. Interflam, Communications Limited, London, 2019: pp. 145–155.

[6] K. Nguyen, P. Weerasinghe, P. Mendis, T. Ngo, J. Barnett, Performance of modern building facades in fire: a comprehensive review, Electron. J. Struct. Eng. 16 (2016) 69–86. http://www.ejse.org/Archives/Fulltext/2016-1/2016-1-8.pdf.

[7] M. Jelčić Rukavina, M. Carević, I. Banjad Pečur, Fire Protection of facades, 2017. https://www.grad.unizg.hr/images/50014277/Fire Protection of Facades.pdf.

[8] B.-G. Branisteanu-Albulescu, Fire Safety of Facades, Lund University, 2019.

[9] P. Van Hees, Development of full-scale façade tests in ISO TC92, (2016).

[10] I. Kotthoff, J. Riemesch-Speer, Mechanism of fire spread on facades and the new Technical Report of EOTA “large-scale fire performance testing of external wall cladding systems,” MATEC Web Conf. 9 (2013). https://doi.org/10.1051/matecconf/20130902010.

[11] S. Colwell, T. Baker, Fire performance of external thermal insulation for walls of multistorey buildings, 2013.

[12] N. White, M. Delichatsios, M. Ahrens, A. Kimball, Fire hazards of exterior wall assemblies containing combustible components, 2013. https://doi.org/10.1051/matecconf/20130902005.

[13] J. Falk, K. Sandin, Ventilated rainscreen cladding: Measurements of cavity air velocities, estimation of air change rates and evaluation of driving forces, Build. Environ. 59 (2013) 164–176. https://doi.org/10.1016/j.buildenv.2012.08.017.

[14] J. Geir, Fire spread modes and performance of fire stops in vented façade constructions – overview and standardization, (2013).

[15] M.P. Giraldo, A. Lacasta, J. Avellaneda, C. Burgos, Computer-simulation study on fire

behaviour in the ventilated cavity of ventilated façade systems, MATEC Web Conf. 9 (2013). https://doi.org/10.1051/matecconf/20130903002.

[16] E.K. Asimakopoulou, D.I. Kolaitis, M.A. Founti, Experimental investigation of the " Ventilated Façade " system performance under fire conditions, (2016) 1–13.

[17] D.I. Kolaitis, E.K. Asimakopoulou, M.A. Founti, A full-scale fire test to investigate the fire behaviour of the "'ventilated facade'" system, Proc. 14th Int. Fire Eng. Conf. Interflam. 2 (2016) 1127–1138.

[18] D. Bikas, K. Tsikaloudaki, K.J. Kontoleon, C. Giarma, S. Tsoka, D. Tsirigoti, Ventilated Facades: Requirements and Specifications Across Europe, Procedia Environ. Sci. 38 (2017) 148–154. https://doi.org/10.1016/j.proenv.2017.03.096.

[19] H. Mattila, Moisture Behavior of Building Insulation Materials and Good Building Practices, Build. Phys. (2017).

[20] G. Agarwal, Evaluation of the Fire Performance of Aluminium Composite Material (ACM) assemblies using ANSI/FM 4880, (2017).

[21] K. Livkiss, Fires in Narrow Construction Cavities, Lund University, 2020.

[22] V. Dréan, B. Girardin, E. Guillaume, T. Fateh, Numerical simulation of the fire behaviour of façade equipped with aluminium composite material-based claddings—Model validation at intermediate scale, Fire Mater. 43 (2019) 839–856. https://doi.org/10.1002/fam.2745.

[23] A. Čolić, I.B. Pečur, Influence of Horizontal and Vertical Barriers on Fire Development for Ventilated Façades, Fire Technol. (2020). https://doi.org/10.1007/s10694-020-00950-w.

[24] EN 13501-1:2018. Fire classification of construction products and building elements - Part 1: Classification using data from reaction to fire tests., 2018.

[25] T.R. Hull, D. Brein, A.A. Stec, Quantification of toxic hazard from fires in buildings, J. Build. Eng. 8 (2016) 313–318. https://doi.org/10.1016/j.jobe.2016.02.014.

[26] BSI Standards Publication Fire classification of construction products and building elements, (2018).

[27] A. Vukadinovi, J. Radosavljevi, Fire safety of exterior façade materials and systems for energy efficiency of buildings, Požární Ochr. (2017) 11–15. https://www.researchgate.net/publication/311743768_Fire_safety_of_exterior_facade_materials_and_systems_for_energy_efficiency_of_buildings.

[28] H. Government, Fire safety APPROVED DOCUMENT B, 2: Buildin (2010) 119. https://doi.org/http://doi.acm.org.libproxy1.nus.edu.sg/10.1145/1822309.1822326.

[29] M. Strömgren, J. Albrektsson, A. Johansson, E. Almgren, Comparative analysis of façade regulations in the Nordic countries, MATEC Web Conf. 9 (2013). https://doi.org/10.1051/matecconf/20130901003.

[30] M. Pfundstein, R. Gellert, M. Spitzner, A. Rudolphi, Types of insulating material, Insul. Mater. (2013). https://doi.org/10.11129/detail.9783034614757.16.

[31] J.P. Hidalgo, S. Welch, J.L. Torero, Performance criteria for the fire safe use of thermal insulation in buildings, Constr. Build. Mater. 100 (2015) 285–297. https://doi.org/10.1016/j.conbuildmat.2015.10.014.

[32] J. Sierra-Pérez, J. Boschmonart-Rives, X. Gabarrell, Environmental assessment of façade-building systems and thermal insulation materials for different climatic conditions, J. Clean. Prod. 113 (2016) 102–113. https://doi.org/10.1016/j.jclepro.2015.11.090.

[33] M. Pfundstein, R. Gellert, M. Spitzner, A. Rudolphi, M. Pfundstein, Properties of insulating materials, Insul. Mater. (2013). https://doi.org/10.11129/detail.9783034614757.8.

[34] P. Kosi, R. Wójcik, An Impact of Air Permeability on Heat Transfer through Partitions Insulated with Loose Fiber Materials The impact of air permeability on heat transfer through partitions insulated with loose fibre materials, (2016). https://doi.org/10.4028/www.scientific.net/AMM.861.190.

[35] N.F. Shahedan, M.M.A.B. Abdullah, N. Mahmed, A. Kusbiantoro, M. Binhussain, S.N. Zailan, Review on thermal insulation performance in various type of concrete, AIP Conf. Proc. 1835 (2017). https://doi.org/10.1063/1.4981868.

[36] M. Jerman, R. Černý, Effect of moisture content on heat and moisture transport and storage properties of thermal insulation materials, Energy Build. 53 (2012) 39–46. https://doi.org/10.1016/j.enbuild.2012.07.002.

[37] S. Schiavoni, F.D. Alessandro, F. Bianchi, F. Asdrubali, Insulation materials for the building sector : A review and comparative analysis, Renew. Sustain. Energy Rev. 62 (2016) 988–1011. https://doi.org/10.1016/j.rser.2016.05.045.

[38] P. Johansson, A. Donarelli, P. Strandberg, Performance of insulation materials for historic buildings, (2018) 80–88.

[39] HM Government, Approved Document L2B: Conservation of fuel and power in existing buildings other than dwellings, Build. Regullations 2010. (2010). https://www.gov.uk/government/uploads/system/uploads/attachment_data/file/540329/BR_PDF_AD_L2B_2013_with_2016_amendments.pdf.

[40] C. Tseng, K. Kuo, Thermal radiative properties of phenolic foam insulation, 4073 (2018). https://doi.org/10.1016/S0022-4073(01)00129-7.

[41] J.P. Hidalgo, J.L. Torero, S. Welch, Fire performance of charring closed-cell polymeric insulation materials: Polyisocyanurate and phenolic foam, Fire Mater. 42 (2018) 358–373. https://doi.org/10.1002/fam.2501.

[42] A. Karamanos, S. Hadiarakou, A.M. Papadopoulos, The impact of temperature and moisture on the thermal performance of stone wool, 40 (2008) 1402–1411. https://doi.org/10.1016/j.enbuild.2008.01.004.

[43] M. Bomberg, T. Kisilewicz, 5.4 Water Resistive Barriers (Wrb), (2017).

[44] R. Lepage, J. Lstiburek, Moisture Durability with Vapor-Permeable Insulating Sheathing, (2013).

[45] G. Agarwal, Y. Wang, S. Dorofeev, Fire performance evaluation of cladding wall assemblies using the 16-ft high parallel panel test method of ANSI/FM 4880, in: Proc. 15th Int. Fire Sci. Eng. Conf. Interflam, Communications Limited, London, 2019: pp. 199–212.

[46] S.T. McKenna, N. Jones, G. Peck, K. Dickens, W. Pawelec, S. Oradei, S. Harris, A.A. Stec, T.R. Hull, Fire behaviour of modern façade materials – Understanding the Grenfell Tower fire, J. Hazard. Mater. 368 (2019) 115–123. https://doi.org/10.1016/j.jhazmat.2018.12.077.

[47] E. Guillaume, S. Ukleja, R. Schillinger, R. Chiva, Study of fire behaviour of facade mock - ups equipped with aluminium composite material - based claddings , using intermediate - scale test method, (2018) 1–17. https://doi.org/10.1002/fam.2635.

[48] W. Government, Use of High Pressure Laminate Panels in external wall systems, 2018.

[49] Exploring the Surface: The Technical Side of Laminate, (n.d.). http://www.iida.org/content.cfm/exploring-the-surface-the-technical-side-of-laminate (accessed February 20, 2020).

[50] T. Gorzelańczyk, K. Schabowicz, Effect of freeze-thaw cycling on the failure of fibre-cement boards, assessed using acoustic emission method and artificial neural network, Materials (Basel). 12 (2019). https://doi.org/10.3390/ma12132181.

[51] R. External, F. Classifications, Fibre cement: the new choice for contemporary construction, 2016.

[52] J. Anderson, L. Bostrom, R. Chiva, E. Guillaume, S. Colwell, A. Hofmann, P. Toth, European approach to assess the fire performance of facades, in: Proc. 15th Int. Fire Sci. Eng. Conf. Interflam, Communications Limited, London, 2019: pp. 213–227.

[53] J. Anderson, L. Boström, R. Jansson, Fire Safety of Façades, 2017.

[54] E. Martinsson, To evaluate fire properties of a facade : - a study on semi natural test methods, Lulea University of Technology, 2018. http://www.diva-portal.org/smash/record.jsf?pid=diva2%3A1193777&dswid=-7755.

[55] E. Guillaume, T. Fateh, R. Schillinger, R. Chiva, S. Ukleja, R. Weghorst, Intermediate-Scale Tests of Ventilated Facades with Aluminium-Composite Claddings, J. Phys. Conf. Ser. 1107 (2018). https://doi.org/10.1088/1742-6596/1107/3/032007.

[56] T. Hakkarainen, Studies on fire safety assessment of construction products, Technical research centre of Finland, 2002.

[57] K. Livkiss, S. Svensson, B. Husted, P. Van Hees, Flame Heights and Heat Transfer in Facade system ventilation cavities, Fire Technol. (2018). https://doi.org/10.1007/s10694-018-0706-2.

[58] B. Karlsson, G.J. Quintiere, Enclosure Fire Dynamics, pp 42, 2000.

[59] C. Huggett, Estimation of rate of heat release by means of oxygen consumption measurements, Fire Mater. 4 (1980) 61–65. https://doi.org/10.1002/fam.810040202.

[60] G.T. Tamura, A.. Wilson, Pressure differences for a nine-storey building as a result of chimney effect and ventilation system operation, (1966).

[61] K.K. Choi, W. Taylor, Combustibility of insulation in cavity walls, J. Fire Sci. 2 (1984) 179–188. https://doi.org/10.1177/073490418400200303.

[62] J. Carlsson, Computational strategies in flame-spread modelling involving wooden surfaces- An evaluation study, Fire Saf. Eng. (2003).

[63] M.J. Hurley, D. Gottuk, J.R.H. Jr., K. Harada, E. Kuligowski, M. Puchovsky, J. Torero, J.M.W. Jr., C. Wieczorek, SFPE Handbook of Fire Protection Engineering (5th Edition), in: Fire Saf. J., 2016: pp. 42–1147. https://doi.org/10.1016/S0379-7112(97)00022-2.

[64] F.B. Mohd Faudzi, Flame Propagation Between Flat Roofing and Photovoltaic Installations, The University of Edinburgh, 2019.

[65] R. Bryant, C. Womeldorf, E. Johnsson, T. Ohlemiller, Radiative heat flux measurement uncertainty, Fire Mater. 27 (2003) 209–222. https://doi.org/10.1002/fam.822.

[66] M. Foley, D.D. Drysdale, Heat transfer from flames between vertical parallel walls, Fire Saf. J. 24 (1995) 53–73. https://doi.org/10.1016/0379-7112(94)00033-C.

[67] J.L. De Ris, L. Orloff, Flame heat transfer between parallel panels, Fire Saf. Sci. (2005) 999–1010. https://doi.org/10.3801/IAFSS.FSS.8-999.

[68] H. Ingason, Fire Experiments in a Two Dimensional Rack Storage, SP Rapport 1993:56, Sp Rep. 56 (1993) 1–25.

[69] F. Vermina Plathner, Limiting conditions for a sustained flame over condensed fuels Analysis by experiments and stagnant layer theory, Lund University, 2020.

[70] J.P. Hidalgo, J.L. Torero, S. Welch, Experimental Characterisation of the Fire Behaviour of Thermal Insulation Materials for a Performance-Based Design Methodology, Fire Technol. 53 (2017) 1201–1232. https://doi.org/10.1007/s10694-016-0625-z.

[71] G. Bytskov, Numerical simulation of fire performance and test conditions for façade insulation materials, 2015. https://doi.org/10.1006/nbdi.1999.0275.

[72] A.M. Papadopoulos, State of the art in thermal insulation materials and aims for future developments, Energy Build. 37 (2005) 77–86. https://doi.org/10.1016/j.enbuild.2004.05.006.

[73] J. Sjöström, R. Jansson, Measuring thermal material properties for structural fire engineering, 15th Int. Conf. Exp. Mech. (2012). http://www.researchgate.net/publication/259357652_MEASURING_THERMAL_MATERIAL_PROPERTIES_FOR_STRUCTURAL_FIRE_ENGINEERING/file/9c96052b2ca177d7d3.pdf.

[74] M. Janssens, C. Gomez, Convective heat transfer in the cone Calorimeter, in: 20th Annu. Conf. Recent Adv. Flame Retard. Polym. Mater. 2009, 2009: pp. 323–335.

[75] D. Drysdale, An Introduction to fire dynamics, pp 66-264, 2011.

[76] G.-Z. Lu, X.-N. Chen, L.-J. Zhou, X.-J. Ding, J.-T. He, Study on modified phenolic foam for Insulation of building's exterior wall, (2015) 73–78. https://doi.org/10.2991/icmra-15.2015.15.

[77] D. Schroer, M. Hudack, M. Soderquist, I. Beulich, Rigid polymeric foam boardstock technical assessment, Annu. Tech. Conf. - ANTEC, Conf. Proc. 3 (2012) 1982–1988.

[78] M. Günther, A. Lorenzetti, B. Schartel, Fire phenomena of rigid polyurethane foams, Polymers (Basel). 10 (2018). https://doi.org/10.3390/polym10101166.

[79] Mechanical properties of insulating materials, (n.d.). https://www.atg.world/view-article/MECHANICAL PROPERTIES OF INSULATING MATERIALS-26827 (accessed April 24, 2020).

[80] M. Thirumal, D. Khastgir, N.K. Singha, B.. Manjunath, Y.P. Naik, Effect of Foam Density on the Properties of Water Blown Rigid Polyurethane Foam, J. Appl. Polym. Sci. 116 (2010) 2658–2667. https://doi.org/10.1002/app.

[81] Thermal conductivity, specific heat capacity and density, (n.d.). https://help.iesve.com/ve2018/table_6_thermal_conductivity__specific_heat_capacity_and_density.htm (accessed April 6, 2020).

[82] X. Lu, M. Viljanen, Fibrous insulation materials in building engineering applications, Fibrous Compos. Mater. Civ. Eng. Appl. (2011) 271–305. https://doi.org/10.1533/9780857095583.3.271.

[83] A. Imamovic, Mechanical Properties of Mineral Stone Wool Fibers Based on Mixture of Blast Furnace Slag and Diabase., Int. J. Adv. Res. 7 (2019) 1408–1413. https://doi.org/10.21474/ijar01/8967.

[84] K. Livkiss, B. Andres, A. Bhargava, P. van Hees, Characterization of stone wool properties for fire safety engineering calculations, J. Fire Sci. 36 (2018) 202–223. https://doi.org/10.1177/0734904118761818.

[85] Mineral wool, (n.d.). https://www.sciencedirect.com/topics/materials-science/mineral-wool (accessed May 7, 2020).

[86] B. Andres, K. Livkiss, J.P. Hidalgo, P. van Hees, L. Bisby, N. Johansson, A. Bhargava, Response of stone wool–insulated building barriers under severe heating exposures, J. Fire Sci. 36 (2018) 315–341. https://doi.org/10.1177/0734904118783942.

[87] R. Ripke, D. Version, The fire performance of steel faced insulation panels with stone wool or polymer cores, Technical University of Denmark, 2018.

[88] M. Uv-fr, M. Ultra, Productinformatie MorgoFassade, (n.d.).

[89] S. Amin, M. Amin, Thermoplastic elastomeric (TPE) materials and their use in outdoor

electrical insulation, Rev. Adv. Mater. Sci. 29 (2011) 15–30.

[90] R. Leisted, Experimental Study of the Effects of Flame Retardants Applied to Chipboard, Technical University of Denmark, 2011.

[91] BSI Standards Publication ISO 5660-2:3025. Reaction-to-fire tests — Heat release, smoke production and mass loss rate, 2019.

[92] Cone calorimeter, (n.d.). http://fr.polymerinsights.com/testing/flammability/cone-calorimeter (accessed April 6, 2020).

[93] Cone calorimeter, (n.d.). https://www.sciencedirect.com/topics/engineering/cone-calorimeter (accessed April 20, 2020).

[94] M.L. Janssens, Improved method for analyzing ignition data from the Cone Calorimeter in the vertical orientation, Fire Saf. Sci. (2003) 803–814. https://doi.org/10.3801/IAFSS.FSS.7-803.

[95] M. Janssens, C. Gomez, Convective heat transfer in the cone calorimeter revisited, 20th Annu. Conf. Recent Adv. Flame Retard. Polym. Mater. 2009. (2009) 323–335.

[96] R. Chen, S. Lu, C. Li, Y. Ding, B. Zhang, S. Lo, Correlation analysis of heat flux and cone calorimeter test data of commercial flame-retardant ethylene-propylene-diene monomer (EPDM) rubber, J. Therm. Anal. Calorim. 123 (2016) 545–556. https://doi.org/10.1007/s10973-015-4900-x.

[97] E. Barreira, E. Bauer, N. Mustelier, F. V.P., Measurement of materials emissivity – Influence of the procedure, 13th Int. Work. Adv. Infrared Technol. Appl. (2015) 242–245.

[98] K-Roc Rainscreen Slab, (n.d.). https://www.kingspan.com/gb/en-gb/products/architectural-facade-systems/rainscreen-substructure/k-roc-rainscreen-slab (accessed April 13, 2020).

[99] P. Blomqvist, M. Hjohlman, Fire tests with textile membranes on the market - results and method development of cone calorimeter and SBI test methods, 2010.

[100] ThermoWorks: Emissivity Table, (n.d.). https://www.optotherm.com/emiss-table.htm (accessed April 19, 2020).

[101] Optotherm: Emissivity values, (n.d.). https://www.optotherm.com/emiss-table.htm (accessed April 19, 2020).

[102] ISO 11697:2012. Reaction to fire tests for façades - Part 1: Intermediate scale test, 2002.

[103] ISO 13785-2:2002 Reaction to fire tests for facades - Part 2: Large-scale test, (n.d.). https://www.iso.org/standard/22928.html (accessed March 7, 2020).

[104] ISO 24473:2008 Fire tests - Open calorimetry, (n.d.). https://www.iso.org/standard/42247.html (accessed April 5, 2020).

[105] RCM Y-Wall Board, (n.d.). https://www.ccfltd.co.uk/RCM-Y-Wall-Board-2400mm-x-1200mm/p/9000218745 (accessed April 28, 2020).